

# A common allele of *HLA* is associated with asymptomatic SARS-CoV-2 infection

<https://doi.org/10.1038/s41586-023-06331-x>

Received: 10 October 2022

Accepted: 15 June 2023

Published online: 19 July 2023

Open access



Danillo G. Augusto<sup>1,2,3,18</sup>, Lawton D. Murdolo<sup>4,18</sup>, Demetra S. M. Chatzileontiadou<sup>4,5,18</sup>, Joseph J. Sabatino Jr<sup>1</sup>, Tasneem Yusufali<sup>1</sup>, Noah D. Peyser<sup>6</sup>, Xochitl Butcher<sup>6</sup>, Kerry Kizer<sup>1</sup>, Karoline Guthrie<sup>1</sup>, Victoria W. Murray<sup>7</sup>, Vivian Pae<sup>7</sup>, Sanmidhi Sarvadhanabhatla<sup>7</sup>, Fiona Beltran<sup>7</sup>, Gurjot S. Gill<sup>7</sup>, Kara L. Lynch<sup>8</sup>, Cassandra Yun<sup>8</sup>, Colin T. Maguire<sup>9</sup>, Michael J. Peluso<sup>7</sup>, Rebecca Hoh<sup>7</sup>, Timothy J. Henrich<sup>10</sup>, Steven G. Deeks<sup>7</sup>, Michelle Davidson<sup>11</sup>, Scott Lu<sup>12</sup>, Sarah A. Goldberg<sup>12</sup>, J. Daniel Kelly<sup>12,13</sup>, Jeffrey N. Martin<sup>12</sup>, Cynthia A. Vierra-Green<sup>14</sup>, Stephen R. Spellman<sup>14</sup>, David J. Langton<sup>15</sup>, Michael J. Dewar-Oldis<sup>4</sup>, Corey Smith<sup>16</sup>, Peter J. Barnard<sup>4</sup>, Sulgi Lee<sup>7</sup>, Gregory M. Marcus<sup>6</sup>, Jeffrey E. Olgin<sup>6</sup>, Mark J. Pletcher<sup>12,17</sup>, Martin Maiers<sup>14</sup>, Stephanie Gras<sup>4,5,19</sup> & Jill A. Hollenbach<sup>1,12,19</sup>

Studies have demonstrated that at least 20% of individuals infected with SARS-CoV-2 remain asymptomatic<sup>1–4</sup>. Although most global efforts have focused on severe illness in COVID-19, examining asymptomatic infection provides a unique opportunity to consider early immunological features that promote rapid viral clearance. Here, postulating that variation in the human leukocyte antigen (*HLA*) loci may underly processes mediating asymptomatic infection, we enrolled 29,947 individuals, for whom high-resolution *HLA* genotyping data were available, in a smartphone-based study designed to track COVID-19 symptoms and outcomes. Our discovery cohort ( $n = 1,428$ ) comprised unvaccinated individuals who reported a positive test result for SARS-CoV-2. We tested for association of five *HLA* loci with disease course and identified a strong association between *HLA-B\*15:01* and asymptomatic infection, observed in two independent cohorts. Suggesting that this genetic association is due to pre-existing T cell immunity, we show that T cells from pre-pandemic samples from individuals carrying *HLA-B\*15:01* were reactive to the immunodominant SARS-CoV-2 S-derived peptide NQKLIANQF. The majority of the reactive T cells displayed a memory phenotype, were highly polyfunctional and were cross-reactive to a peptide derived from seasonal coronaviruses. The crystal structure of *HLA-B\*15:01*–peptide complexes demonstrates that the peptides NQKLIANQF and NQKLIANAF (from OC43-CoV and HKU1-CoV) share a similar ability to be stabilized and presented by *HLA-B\*15:01*. Finally, we show that the structural similarity of the peptides underpins T cell cross-reactivity of high-affinity public T cell receptors, providing the molecular basis for *HLA-B\*15:01*-mediated pre-existing immunity.

Despite some inconsistent reporting of symptoms<sup>1</sup>, studies have shown that at least 20% of individuals infected with severe acute respiratory syndrome coronavirus 2 (SARS-CoV-2) remain asymptomatic<sup>2–4</sup>. The examination of asymptomatic infection provides a unique opportunity to consider early disease and immunological features that promote rapid viral clearance. Specific focus on asymptomatic infection has the potential to further our understanding of disease pathogenesis and supports ongoing efforts towards vaccine development and the identification of potential therapeutic targets.

It remains unclear why many individuals successfully clear infection without major complications while others develop severe disease, even without known risk factors for severe COVID-19 outcomes<sup>5</sup>. However, host genetics is known to be implicated in differential immunological responses to infection and disease progression. Numerous studies

intending to understand the genetic basis of differential outcomes in COVID-19 have been underway since nearly the start of the global pandemic, including the multicentre Host Genetics Initiative<sup>6</sup>. However, the vast majority of these studies have examined genetic associations with severe disease course, in primarily hospitalized cohorts<sup>7,8</sup>. As a result, although most individuals infected with SARS-CoV-2 experience mild disease course or are entirely asymptomatic, very few studies have examined genetics in the context of non-hospitalized, prospective, community-based cohorts.

The human leukocyte antigen (*HLA*) region (6p21) is the most polymorphic and medically important human genomic region. Variation in *HLA* has been associated with hundreds of diseases and conditions, including infection. Among the many genes involved in human immune responses, *HLA* variants have among the strongest associations with

# Article

**Table 1 | HLA-B\*15:01 is associated with asymptomatic SARS-CoV-2 infection**

	Asymptomatic	Symptomatic				
	cf	cf	OR	95% CI	P	$P_{adj}$
<b>Discovery cohort</b>						
HLA-B*15:01	0.199	0.094	2.40	1.54–3.64	$5.67 \times 10^{-5}$	0.002
HLA-B*15:01/15:01	0.022	0.005	8.58	1.74–34.43	0.001	
<b>UK cohort</b>						
HLA-B*15:01	0.171	0.070	3.56	1.15–10.97	0.02	
<b>CHIRP/LIINC cohort</b>						
HLA-B*15:01	0.250	0.086	3.44	0.50–23.64	0.13	

Results are shown for two-sided tests based on a generalized linear model, including adjustment for sex and age. cf, carrier frequency. The ORs are relative to non-HLA-B\*15:01 carriers.

viral infections. For example, *HLA* is associated with rapid progression and viral load control of human immunodeficiency virus (HIV)<sup>9</sup>, hepatitis B, hepatitis C and other infectious diseases<sup>10</sup>. Notably, *HLA* class I and class II alleles have also been associated with the severe acute respiratory syndrome caused by SARS-CoV<sup>11–13</sup>.

In silico analyses have pointed to *HLA* as relevant molecules for SARS-CoV-2 risk and essential targets for vaccine development<sup>14–17</sup>. For example, HLA-B\*46:01 has low predicted binding to peptides of SARS-CoV-2, suggesting that individuals expressing this molecule may be more vulnerable to COVID-19<sup>16</sup>, corroborating previous results showing *HLA-B\*46:01* association with SARS risk<sup>12</sup>. By contrast, HLA-B\*15:03 was predicted to protect against COVID-19 by presenting highly conserved SARS-CoV-2 peptides to T cells<sup>16</sup>. More recently, it was demonstrated that, although there is some overlap, many SARS-CoV-2 epitopes for CD8<sup>+</sup> T cells are *HLA* specific<sup>16</sup>. To date, relatively few studies have directly examined *HLA* associations with infection, with mixed and inconclusive results in relatively small cohorts<sup>18–20</sup>. Larger studies that relied on genome-wide data to impute *HLA* did not find robust associations with disease<sup>7,21</sup>; however, these studies focused primarily on hospitalized patients with a severe disease course.

Understanding the impact of *HLA* variation in disease promises to provide meaningful insights that are relevant to understanding the immunopathogenesis of COVID-19, while informing vaccine development and potential immunotherapies. Here we present a large study directly examining *HLA* variation in the context of primarily mild disease. We invited volunteer bone marrow donors, from whom high-resolution *HLA* genotyping data were already available, to participate in the COVID-19 Citizen Science Study—a smartphone-based study designed to track COVID-19 symptoms and outcomes, including self-reported positive tests for SARS-CoV-2 infection, to develop a prospective cohort currently comprising nearly 30,000 individuals, as well as two additional independent cohorts. We further contextualize our findings by examining T cell reactivity, T cell receptor repertoire, affinity and structural implications for the observed *HLA* associations. Our results provide strong support for the role of *HLA* class I in viral clearance leading to asymptomatic infection among individuals with SARS-CoV-2 infection and provide an important framework for additional studies aimed at revealing the immunological and genetic basis for recovery from SARS-CoV-2 infection.

## HLA-B\*15:01 in asymptomatic COVID-19

Our final cohort comprised 1,428 individuals who reported a positive test for active SARS-CoV-2 infection and self-identified as white. Basic demographics for all individuals are given in Extended Data Table 1. The full list of reported diseases and conditions and their frequency in this cohort is given in Supplementary Table 1. To identify whether *HLA* variation affects the likelihood of an individual remaining asymptomatic after SARS-CoV-2 infection, we analysed high-resolution genotyping

data for five highly polymorphic *HLA* class I and class II genes (*HLA-A*, *HLA-B*, *HLA-C*, *HLA-DRB1*, *HLA-DQB1*).

We found that the allele *HLA-B\*15:01* was significantly overrepresented in asymptomatic individuals relative to symptomatic individuals (frequency = 0.1103 versus 0.0495, odds ratio (OR) = 2.38, 95% confidence interval (CI) = 1.51–3.65,  $P = 3 \times 10^{-5}$ , Bonferroni-corrected  $P(P_{adj}) = 0.002$ ). No other *HLA* allele at any locus was significantly associated after correction for multiple comparisons. Allele frequencies for all loci are provided in Supplementary Table 2.

To adjust for the effect of comorbid conditions, as well as sex and age differences, we fitted a series of regression models but did not find any effect of patient-reported comorbidities on the likelihood of asymptomatic disease. Thus, our final model was adjusted only for age and sex, again showing a significant association of *HLA-B\*15:01* with asymptomatic infection after adjustment for these variables (OR = 2.40, 95% CI = 1.54–3.64,  $P = 5.67 \times 10^{-5}$ ,  $P_{adj} = 0.003$ ; Table 1).

Finally, we observed a strong additive effect for the associated genotype. Individuals carrying two copies of *HLA-B\*15:01* are more than eight times more likely to remain asymptomatic than individuals carrying other genotypes (OR = 8.58, 95% CI = 1.74–34.43,  $P = 0.001$ ). Overall, one in five individuals (20%) who remained asymptomatic after infection carried *HLA-B\*15:01*, compared with 9% among patients reporting symptoms.

## HLA-DRB1\*04:01 enhances HLA-B\*15:01

To understand whether additional *HLA* alleles might interact with *HLA-B\*15:01* in asymptomatic infection, we tested all pairwise two-locus haplotypes containing *HLA-B*. Overall, haplotypic associations for *HLA-B-HLA-DRB1* and *HLA-A-HLA-B* were found to be significant at  $P = 0.01$ . Examining specific allelic haplotypes, these associations were driven by two *HLA-B\*15:01* haplotypes: *HLA-B\*15:01-HLA-DRB1\*04:01* and *HLA-A\*02:01-HLA-B\*15:01* (Supplementary Tables 3 and 4).

After adjusting for sex and age, only the combination of *HLA-B\*15:01* and *HLA-DRB1\*04:01* remained significant after correction for multiple comparisons ( $P = 3 \times 10^{-4}$ ,  $P_{adj} = 0.01$ ). We found an OR for this combination (OR = 3.17, 95% CI = 1.65–5.80) that exceeds that for *HLA-B\*15:01* alone, suggesting that, although not significantly associated with the asymptomatic infection on its own in this cohort, the class II allele *HLA-DRB1\*04:01* enhances the effect of *HLA-B\*15:01*.

## Replication in independent cohorts

To confirm our findings, we examined two independent cohorts of patients with European ancestry. We first undertook a reanalysis of the primary *HLA* genotype data in a UK cohort that was previously reported<sup>22</sup>; *HLA-B\*15:01* was not examined with respect to asymptomatic infection owing to its marginal significance in their analyses. Testing only the allele of interest, we found that *HLA-B\*15:01* is strongly

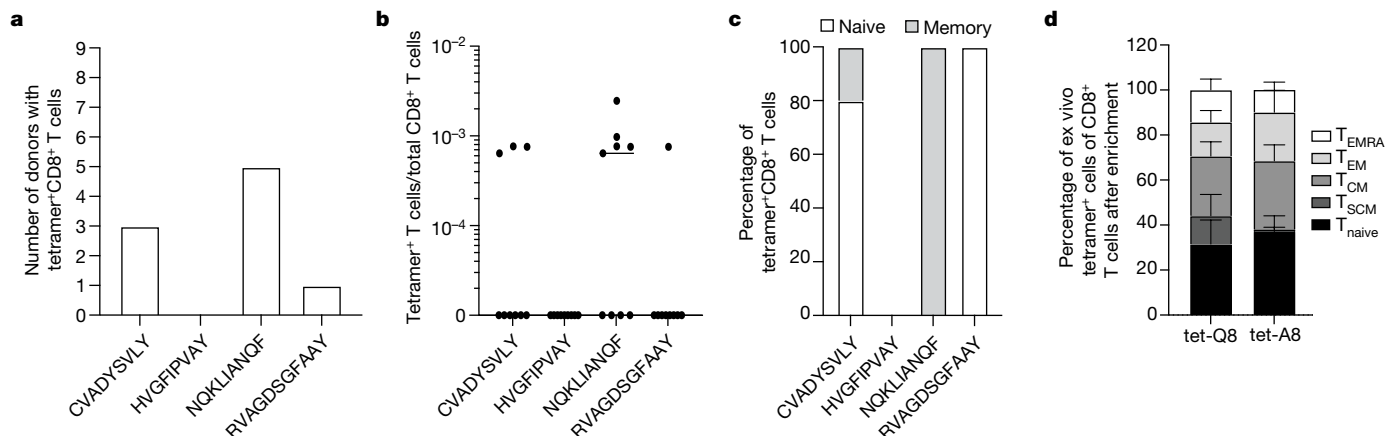


**Fig. 1 | T cell reactivity in pre-pandemic samples from individuals carrying HLA-B\*15:01.** **a–c**, Ex vivo combinatorial tetramer analysis for the four indicated peptides was performed in nine pre-pandemic donor samples. **a, b**, The number of donors with detectable tetramer<sup>+</sup> CD8<sup>+</sup> T cells (**a**) and their frequencies (**b**) are shown. **c**, The proportion of naive (CD45RA<sup>+</sup>CCR7<sup>+</sup>) and memory (combination of CD45RA<sup>+</sup>CCR7<sup>−</sup>, CD45RA<sup>−</sup>CCR7<sup>+</sup>, CD45RA<sup>−</sup>CCR7<sup>−</sup>) cells among tetramer<sup>+</sup> CD8<sup>+</sup> T cells (based on  $n = 9$  samples). **d**, Phenotypic

analysis after TAME of ex vivo tetramer<sup>+</sup> NQK-Q8-specific (tet-Q8) and NQK-A8-specific (tet-A8) T cells in 7 and 6 donors, respectively. Cell types were defined as follows: T<sub>naive</sub> (CD45RA<sup>+</sup>CCR7<sup>+</sup>CD95<sup>−</sup>); T<sub>SCM</sub> (stem cell memory, CD45RA<sup>+</sup>CCR7<sup>−</sup>CD95<sup>+</sup>); T<sub>CM</sub> (central memory, CD45RA<sup>−</sup>CCR7<sup>+</sup>); T<sub>EM</sub> (effector memory, CD45RA<sup>−</sup>CCR7<sup>−</sup>); T<sub>EMRA</sub> (terminally differentiated, CD45RA<sup>−</sup>CCR7<sup>−</sup>). Data are mean  $\pm$  s.e.m.

associated with asymptomatic infection in this cohort when adjusting for sex and age ( $P = 0.02$ , OR = 3.56, 95% CI = 1.15–10.94). Similar to our discovery cohort, we found that the carrier frequency for HLA-B\*15:01 was 17% in asymptomatic individuals compared with 7% in symptomatic patients (Table 1).

We next examined the association between HLA-B\*15:01 and asymptomatic infection in the combined UCSF prospective longitudinal COVID-19 Host Immune Response Pathogenesis (CHIRP) and Long-term Impact of Infection with Novel Coronavirus (LIINC) cohort. Here, 12 out of 82 individuals with European ancestry were identified as having an asymptomatic disease course. We found again that the carrier frequency of HLA-B\*15:01 was exceptionally high (25%) in asymptomatic individuals compared with in symptomatic patients (8.6%). Although the power was somewhat limited by the sample size, and therefore cannot be considered to be a fully independent replication, the findings are strongly trending in support of our finding of a strong association of this allele with asymptomatic disease ( $P = 0.13$ , OR = 3.44, 95% CI = 0.50–23.64; Table 1). Finally, a meta-analysis across all three datasets (Citizen Science, UK, CHIRP/LIINC) confirmed the strong and consistent association of HLA-B\*15:01 with asymptomatic infection ( $P < 10^{-4}$ , OR = 2.55, 95% CI = 1.73–3.77; Supplementary Fig. 1).

## Unexposed T cells react to SARS-CoV-2

Owing to their high avidity for their cognate T cell receptors, pHLa (peptide–HLA) tetramers have been systematically used to visualize and quantify low-frequency antigen-specific T cells ex vivo using flow cytometry<sup>23</sup>. We focused on four SARS-CoV-2 epitopes (CVADYSVLY, HVGEIPVAY, NQKLIANQF and RVAGDGSFAAY) that were previously shown to elicit cellular immunity mediated by cytotoxic CD8<sup>+</sup> T cells in patients with COVID-19 carrying HLA-B\*15:01 (refs. 24–28). We next performed ex vivo pHLa tetramer evaluation with the SARS-CoV-2 peptides to detect antigen-specific CD8<sup>+</sup> T cells in nine pre-pandemic peripheral blood mononuclear cell (PBMC) samples. We observed tetramer<sup>+</sup> CD8<sup>+</sup> T cells for three of the SARS-CoV-2 epitopes (Fig. 1a,b, Supplementary Tables 5 and 6 and Supplementary Figs. 2 and 3).

NQKLIANQF (hereafter, NQK-Q8) was detectable in the highest proportion of samples (5 out of 9; 55.6%). Notably, in those donors, 100% of ex vivo NQK-Q8 tetramer<sup>+</sup> CD8<sup>+</sup> T cells were memory T cells, indicating pre-existing T cell immunity against SARS-CoV-2 in a subset

of individuals carrying HLA-B\*15:01 who did not have any previous contact with the virus (Fig. 1c and Supplementary Table 5).

NQK-Q8 was previously identified as immunodominant<sup>28</sup>, and these authors also demonstrated that NQK-Q8-specific T cells from HLA-B\*15:01<sup>+</sup> patients with infection were cross-reactive to the highly homologous peptide NQKLIANAF (hereafter, NQK-A8) from the seasonal coronaviruses HKU1-CoV and OC43-CoV. Given the high level of NQK-Q8-specific memory T cells compared with naive CD8<sup>+</sup> T cells observed in the initial set of pre-pandemic samples that we tested (Fig. 1c), we sought to determine whether the same phenotype was also observed for the peptide NQK-A8 in additional samples from HLA-B\*15:01<sup>+</sup> individuals with no exposure to SARS-CoV-2. We performed ex vivo tetramer magnetic enrichment (TAME) with tetramers of each peptide, NQK-Q8 and NQK-A8, bound to HLA-B\*15:01 (tet-Q8 and tet-A8, respectively) (Fig. 1d, Extended Data Figs. 1 and 2 and Supplementary Fig. 4) using a larger number of additional samples ( $n = 7$  and  $n = 5$  for tet-Q8 and tet-A8, respectively). We used pre-pandemic samples from the USA and Australia according to our previous study<sup>25</sup>. All of these samples exhibited tetramer<sup>+</sup> CD8<sup>+</sup> T cells. Overall, we observed NQK-Q8-specific T cells in 75% of HLA-B\*15:01<sup>+</sup> donors with no previous exposure to SARS-CoV-2 ( $n = 12$  out of 16; Fig. 1a–d and Extended Data Fig. 1).

We next analysed the phenotype of the tetramer<sup>+</sup> CD8<sup>+</sup> T cells for both NQK peptides (Fig. 1d). We observed an abundance of memory T cells specific for NQK-Q8 in pre-pandemic samples (Fig. 1d and Extended Data Fig. 2). A similar phenotypic profile was observed for the NQK-A8-specific T cells, with most tetramer<sup>+</sup> CD8<sup>+</sup> T cells being memory cells (Fig. 1d and Extended Data Fig. 2). The high proportion of effector memory and effector memory re-expressing CD45RA (T<sub>EMRA</sub>) T cells (29% for NQK-Q8 and 31% for NQK-A8) indicates a potent T cell response towards these peptides, which is a desirable characteristic for protective immunity. We were able to detect ex vivo tetramer<sup>+</sup> CD8<sup>+</sup> T cells for NQK-Q8 ( $n = 7$ ) and NQK-A8 ( $n = 6$ ) (Fig. 1d and Extended Data Fig. 1). Overall, our data show the presence of CD8<sup>+</sup> T cells specific for both NQK peptides, with a similar phenotype and magnitude in unexposed donors.

## Cross-reactive NQK-specific T cells

We next sought to determine whether the T cell cross-reactivity observed previously<sup>28</sup> in patients with infection could be observed

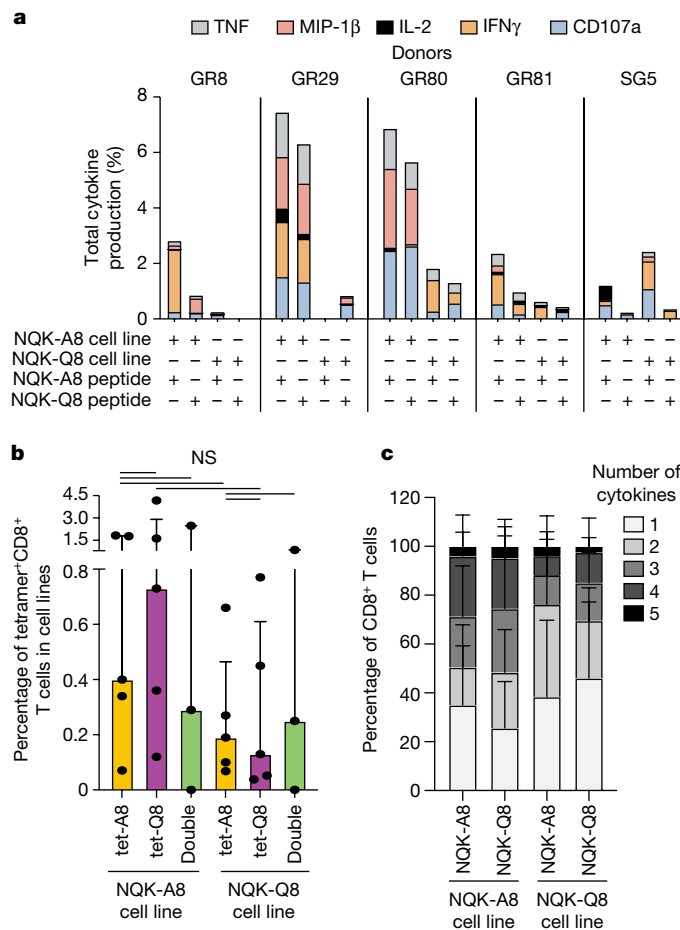


**Fig. 2 | NQK-specific T cells are cross-reactive.** **a**, Total cytokine production by CD8<sup>+</sup> T cells in NQK-A8- and NQK-Q8-specific T cell lines. Each peptide-specific T cell line was restimulated individually with its cognate peptide or the homologous peptide as indicated, and the cytokine response was measured by intracellular cytokine staining ( $n = 5$  donors). Percentages of effector functions (IFN $\gamma$ , TNF, IL-2, MIP-1 $\beta$ , CD107a) minus the no peptide control are reported. **b**, In vitro tetramer analysis for the NQK-Q8- and NQK-A8-specific T cell lines ( $n = 5$  donors). The cell lines were tetramer stained with a single tet-A8 (orange bar) or tet-Q8 (purple bar) tetramer or both tetramers (green bar). The frequency of tetramer<sup>+</sup> CD8<sup>+</sup> T cells is shown. Data are median  $\pm$  interquartile range. Differences between two groups were compared using two-tailed unpaired  $t$ -tests.  $P < 0.05$  was considered to be significant. NS, not significant. **c**, Polyfunctionality analysis of CD8<sup>+</sup> NQK-peptide-specific T cells from five unexposed donors. The number of functions is shown on a scale from 5 (black) to 1 (white). Data are the relative frequency (%) of total cytokine<sup>+</sup> CD8<sup>+</sup> T cells. Data are mean  $\pm$  s.e.m. Differences between two groups were determined using two-tailed unpaired  $t$ -tests.  $P < 0.05$  was considered to be significant, and the result was not significant.

in unexposed individuals. We set up T cell lines with each peptide separately using PBMCs from unexposed and unvaccinated donors ( $n = 5$ , *in vitro*). Each cell line was then restimulated with either peptide. CD8<sup>+</sup> T cell recognition and activation were determined by tetramer staining and intracellular cytokine staining, respectively (Fig. 2a and Supplementary Fig. 4).

All of the cell lines were characterized by the presence of tetramer<sup>+</sup> CD8<sup>+</sup> T cells for both peptides (Supplementary Fig. 5), showing a bidirectional cross-reactivity whereby T cells can recognize both NQK peptides derived from the different viruses. The magnitude of tetramer<sup>+</sup> CD8<sup>+</sup> T cells was different among donors and slightly higher for the cell lines generated with the NQK-A8 peptide (Fig. 2b).

The co-staining of the T cell lines with both tetramers (tet-Q8, allophycocyanin (APC) conjugated; tet-A8, phycoerythrin (PE) conjugated) showed that the vast majority of T cells were cross-reactive (Supplementary Fig. 5).

We subsequently measured the level of T cell responsiveness to each peptide. T cells from all donors, apart from GR8, responded to the cognate peptide (Fig. 2a). In four out of five donors, a stronger response was observed in the NQK-A8-specific cell lines independent of the peptide (Fig. 2a). These findings were similar to what we previously observed for the N(105–113) peptides derived from SARS-CoV-2 and HKU1-CoV/OC43-CoV, in the context of HLA-B\*07:02, whereby the T cells were more strongly stimulated after presentation of the peptide derived from seasonal coronavirus compared with the SARS-CoV-2-derived peptide in unexposed donors<sup>25</sup>.

Notably, although the percentage of cytokine<sup>+</sup> CD8<sup>+</sup> T cells was different between donors (around 0–8%; Fig. 2a), the level and profile of cytokines were comparable for each cell line between the two peptides. This observation suggests that both NQK peptides stimulate T cells at similar magnitudes, which may reflect a high level of T cell cross-reactivity. We next examined the functional profile of the CD8<sup>+</sup> T cells, which corresponds to their ability to exhibit different effector functions (IFN $\gamma$ , TNF, IL-2, MIP-1 $\beta$ , CD107a; Fig. 2c). A highly polyfunctional T cell response, with up to five functions expressed, was observed for both cell lines that were restimulated with either peptide. At least 40% ( $n = 2$  out of 5) and up to 80% ( $n = 4$  out of 5) of donors had T cells exhibiting all five functions in one or more cell line. An average of 2.5–4.7% of CD8<sup>+</sup> T cells exhibited all five functions tested (Fig. 2c and Extended Data Fig. 3).

In summary, the T cell response against NQK peptides from seasonal coronaviruses and SARS-CoV-2 in individuals never exposed to SARS-CoV-2 is highly cross-reactive and polyfunctional.

## NQK-specific T cells express public TCRs

We next determined the T cell receptor (TCR) repertoire specific to both NQK-A8 and NQK-Q8 peptides. Using single-cell sorting of tetramer<sup>+</sup> CD8<sup>+</sup> T cells and TCR sequencing, we obtained 456 productive clonotypic sequences from eight unexposed donors and one triple-vaccinated donor (Supplementary Table 7). The TCR repertoires of T cells specific to each or both NQK peptides (single or double tetramer<sup>+</sup> CD8<sup>+</sup> T cells) were obtained from both T cell lines (*in vitro*) and unstimulated PBMCs (*ex vivo*) (Fig. 3a,b, Supplementary Table 7, Extended Data Figs. 4 and 5 and Supplementary Fig. 6).

The NQK-specific TCR repertoires overlap extensively with shared clonotypes and public TCRs (Supplementary Tables 7 and 8). The *ex vivo* TCR repertoire was strongly biased with clonotypes expressing TRAV9 (31%) or TRAV21 (15%) paired with the dominant TRBV7-2/7-8 (71%) (Fig. 3a,b and Supplementary Table 7). Although the TRBV7-2/7-8 clonotypes were also present in the *in vitro* repertoire, their frequency was decreased (11%); we also observed expansion of the TRBV5-4/5-8<sup>+</sup> (35%), TRBV9<sup>+</sup> (18%) and TRBV20-1<sup>+</sup> (24%) clonotypes. Similarly, a frequency shift for TRAV gene usage was observed in the *in vitro* TCR repertoire with a decrease in TRAV21<sup>+</sup> clonotypes (6%), an absence of TRAV9<sup>+</sup> clonotypes, and the emergence of TRAV19<sup>+</sup> (21%), TRAV38-2/DV8\*01<sup>+</sup> (19%) and TRAV41<sup>+</sup> (47%) clonotypes. The TRAV38-2/DV8\*01<sup>+</sup> and TRAV41<sup>+</sup> clonotypes were expanded in only one donor each (GR81 and GR80, respectively), and these paired only with TRBV20-1 and TRBV5-4/5-8, respectively; these expanded clonotypes were cross-reactive (Supplementary Table 7). The CD8<sup>+</sup> T cells able to bind both tet-A8 and tet-Q8 primarily expressed TRBV7-2/7-8 (42%) paired with TRAV21 (54%); TRBV9 (36%, pairing unknown); or TRBV5-4/5-8 (12%) paired with TRAV41 (36%) (Supplementary Table 7). Moreover, the CDR3 loop length and sequence motifs shared similarities (Fig. 3 and Extended Data Fig. 5). Public TCRs, defined as identical TCRs shared between individuals, were also isolated<sup>29</sup>. The public

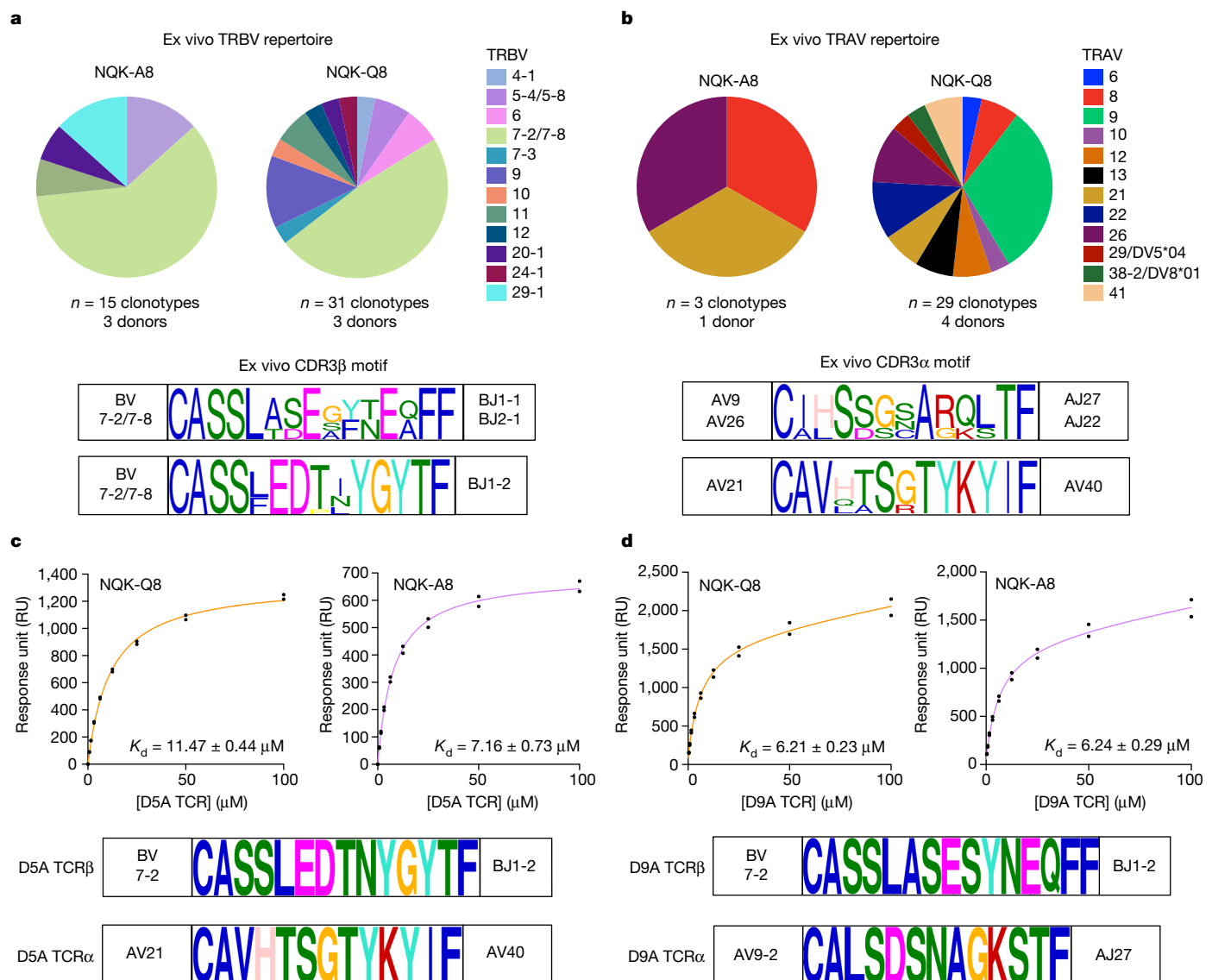


**Fig. 3 | NQK-specific T cells are characterized by the presence of high-affinity public TCRs in unexposed donors.** **a, b**, Analysis of the ex vivo TCR repertoire for NQK-A8- and NQK-Q8-specific T cells after TAME on the basis of TRBV (a) and TRAV (b) use. The pie charts show the percentage of each TRBV or TRAV used in the single-cell sorted clonotypes. The CDR3 $\beta$  and CDR3 $\alpha$  sequence motifs are shown below the pie charts, respectively, for the TCRs with the biased expression of TRBV7-2/7-8 paired with TRAV9/26 or TRAV21, including the public TCRs. **c, d**, The binding response (response units (RU)) of D5A (c) and

D9A (d) TCRs (analyte) against HLA-B\*15:01-NQK complexes (A8 in orange and Q8 in purple). The public TCR D5A expresses TRBV7-2 paired with TRAV21, and the public D9A TCR expresses TRBV7-2 paired with TRAV9-2; the CDR3 $\beta$  and CDR3 $\alpha$  sequences for each public TCRs are shown below the binding curves. The SPR steady-state binding curves represent binding under a TCR concentration range of 0.39–100  $\mu$ M.  $n = 2$  biologically independent experiments performed in duplicate; the graph shows the results from one experiment performed in duplicate, represented by the black dots.

NQK-specific TCRs were TRBV7-2/7-8 $^+$  paired with TRAV21 or TRAV9-2 and were observed both ex vivo and in vitro in unexposed donors (Fig. 3c,d and Supplementary Table 8). These public and cross-reactive TCRs have also been isolated from donors who had recovered from COVID-19 and/or vaccinated donors previously<sup>28</sup> (Supplementary Table 8). This finding shows the potential for a strong pre-existing immune memory pool of cross-reactive public TCRs specific to the NQK peptides that is similar to that observed after infection. The phenotypic profiles of the clonotypes expressing the public TCRs ex vivo in unexposed donors were either stem memory or central memory T cells.

To summarize, the NQK-Q8- and NQK-A8-specific TCR repertoires are biased with the presence of public and cross-reactive TCRs in unexposed donors, comparable to observations in donors who have recovered from COVID-19 and/or vaccinated donors (Supplementary Figs. 6 and 7). These findings suggest that the existence of memory

cross-reactive NQK-specific TCRs before infection could have a critical role in the immune response to SARS-CoV-2, contributing to asymptomatic infection in individuals carrying HLA-B\*15:01.

### NQK peptides share structure similarity

The HLA-B\*15:01-restricted peptide NQK-Q8 is conserved among all SARS-CoV-2 variants, even the new XBB variant of Omicron, and differs by only one amino acid from the HKU1-CoV/OC43-CoV peptide (Supplementary Fig. 8). Importantly, NQK-Q8-reactive T cells from HLA-B\*15:01 $^+$  individuals infected with SARS-CoV-2 were previously shown to be cross-reactive to the homologous peptide from seasonal coronaviruses<sup>28</sup>. As we have shown the presence of pre-existing T cell immunity in pre-pandemic samples and cross-reactivity of the NQK peptide-specific T cells (Figs. 1 and 2), we sought to investigate whether

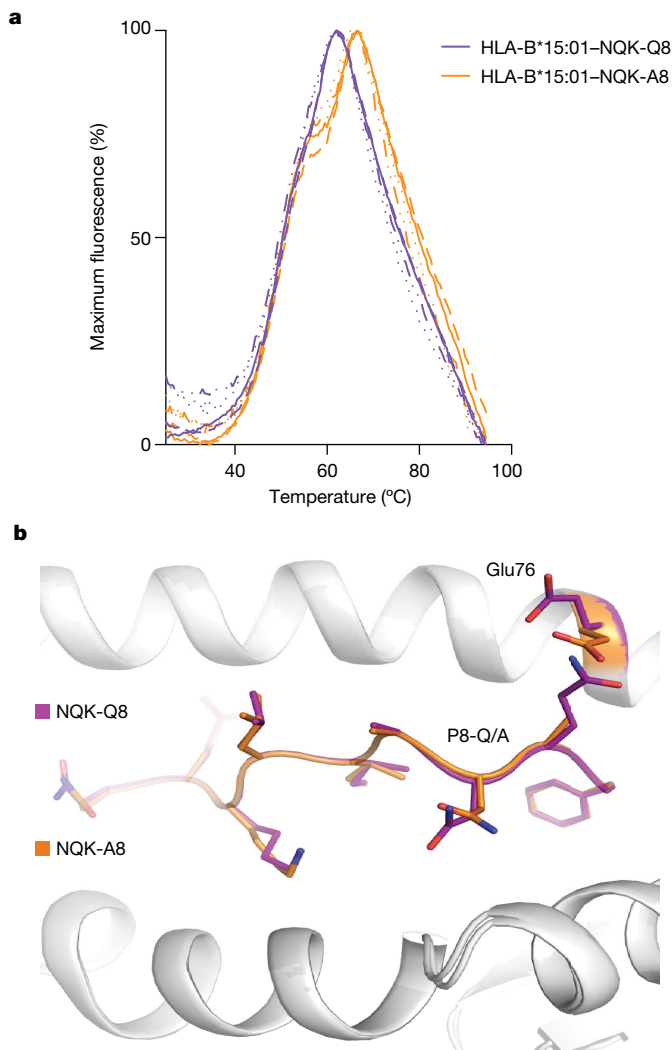


**Fig. 4 | NQK peptides are stable and adopt the same conformation bound to the HLA-B\*15:01 molecule.** **a**, DSF plots showing the normalized fluorescence intensity versus temperature for HLA-B\*15:01 in a complex with the NQK-Q8 (purple) or NQK-A8 (orange) peptide measured at concentrations of 5  $\mu$ M and 10  $\mu$ M.  $n = 2$  biologically independent experiments performed in duplicate, represented by the different lines. **b**, Superimposition of the crystal structures of HLA-B\*15:01 (white cartoon) in a complex with either the NQK-Q8 (purple stick) or the NQK-A8 (orange stick) peptide.

the amino acid change in the NQK peptides from SARS-CoV-2 and the seasonal coronaviruses HKU1-CoV and OC43-CoV affects the stability of HLA-B\*15:01.

We refolded the HLA-B\*15:01 molecule in the presence of each peptide and performed a thermal melt assay using differential scanning fluorimetry (DSF). Both pHHLA complexes exhibited the same thermal melting point ( $T_m$ ; Fig. 4a and Supplementary Table 9), indicating that the Gln>Ala amino acid change does not affect the overall stability of the pHHLA. We crystallized each peptide in a complex with HLA-B\*15:01 and solved their structures at high resolution (Fig. 4b, Extended Data Table 2 and Extended Data Fig. 6). Overall, NQK-Q8 adopted a canonical conformation within the antigen-binding cleft of the HLA-B\*15:01 molecule<sup>30</sup>. The Gln at position 2 (P2) was deeply inserted into the B pocket of HLA-B\*15:01, whereas the P9-Phe primary anchor residue bound to the F pocket. The central part was more mobile than the rest of the peptide (Extended Data Fig. 6). The NQK-Q8 peptide exposed to the solvent, and potentially to circulating T cells, five of its nine residues (P1-Asn, P4-Leu, P6-Ala, P5-Asn and P8-Gln). The NQK-A8 bound

similarly in the HLA-B\*15:01 cleft (Fig. 4b and Extended Data Fig. 6). The superposition of the two pHHLA structures revealed very little difference between the two complexes, with a root mean squared deviation of 0.08 Å for the C $\alpha$  atoms of the antigen-binding cleft (residues 1–180) and 0.12 Å for the peptides. Only some local rearrangement around the P8 of the peptide was observed with a shift of the Glu76 side chain to avoid steric clashes with the P8-Gln (Fig. 4b). This change, which is on the surface of the peptide, could affect T cell interaction and might change the TCR affinity. To test the effect of the P8 difference within the NQK peptides, we selected some representative TCRs to perform affinity measurements using surface plasmon resonance (SPR). We selected the three TRBV7-2<sup>+</sup> public TCRs paired with either TRAV9-2 (D9A TCR) or TRAV21 (A6A and D5A TCRs) (Fig. 3c,d and Supplementary Table 8).

All of the TCRs tested were able to bind with high affinity ( $K_d$  range, 6–20  $\mu$ M) to both the NQK-A8 and NQK-Q8 peptides presented by the HLA-B\*15:01 molecule (Fig. 3c,d, Extended Data Figs. 7 and 8 and Supplementary Table 10). We observed a slower dissociation rate for the two TRAV21<sup>+</sup> TCRs (A6A and D5A TCRs) compared with the TRAV9<sup>+</sup> D9A TCR (Extended Data Fig. 7). The TCRs also differ in their CDR3 $\beta$  loops.

In a previous study<sup>28</sup>, the cross-reactivity of two NQK-Q8-specific TCRs (TCR1 and TCR2) transfected into Jurkat cells was shown. The published TCR1 and TCR2<sup>28</sup> differ by only one residue in each CDR3 loop from A6A and D5A TCRs, respectively (Supplementary Table 8). This is reflected by the similar affinity of the A6A and D5A TCRs for the NQK-A8 and NQK-Q8 peptides observed here (Supplementary Table 10). Overall, our data show that the similar conformation and ability to stabilize the HLA-B\*15:01 molecule of the two NQK peptides underpin the similar affinity observed for the public TCRs. Moreover, the high affinity of these TCRs towards the NQK peptides might trigger a rapid expansion of these memory cells after SARS-CoV-2 infection.

## Discussion

Understanding the biological underpinning of asymptomatic infection with SARS-CoV-2 has important implications for public health measures, vaccine design and therapeutic development. Here we provide evidence of a genetic basis and the mechanistic explanation underlying asymptomatic disease. Leveraging a large database and mobile technology in this crowd-sourced study, we reveal important insights into the immunogenetic underpinnings of asymptomatic SARS-CoV-2 infection. Our use of a mobile application and a pre-existing database for medical research enabled us to screen nearly 30,000 individuals who were previously genotyped for *HLA* for viral infection and disease course. We augment our findings of a strong *HLA* association with asymptomatic disease course in this unique cohort with functional and structural studies to support a model of pre-existing immunity to explain the observed *HLA* association.

We show that, among participants reporting a positive test result for SARS-CoV-2, *HLA-B\*15:01* is significantly associated with asymptomatic infection. We observed that individuals carrying this common allele (approximately 10% in individuals with European ancestry) are more than twice as likely to remain asymptomatic after SARS-CoV-2 infection compared with those who do not, and a notable effect of *HLA-B\*15:01* homozygosity increasing the chance of remaining asymptomatic by more than eight times. This suggests important features of early infection with SARS-CoV-2. Supporting the role of *HLA-B\*15:01* in mediating asymptomatic infection, we found a highly similar frequency distribution of this allele in asymptomatic versus symptomatic patients in two independent cohorts.

Despite a growing number of published studies, the role of *HLA* variation in COVID-19 has remained unclear, with no clear consensus in the literature to date and, notably, few studies examining asymptomatic infection as a primary phenotype<sup>18</sup>. Our reanalysis of the primary data underlying a reported association between *HLA-DRB1\*04:01* and

asymptomatic infection<sup>22</sup> uncovered clear evidence for the role of *HLA-B\*15:01* in asymptomatic disease, which was not reported in the initial study. Although the data in our discovery cohort did not corroborate the association for *HLA-DRB1\*04:01* alone, we did find that this allele enhanced the effect of *HLA-B\*15:01* when the pair were in combination. Note that this is the *HLA-DRB1* allele that is most commonly associated with *HLA-B\*15:01* in individuals in the United States who self-identify as white<sup>31</sup> and it is therefore difficult to differentiate a real effect from one related to linkage disequilibrium between these loci unless directly tested. Similarly, another recent paper describing an association of *HLA-DRB1* alleles with asymptomatic infection did not genotype for *HLA-B*<sup>32</sup>. Finally, two other large studies that used patient questionnaires regarding symptoms did not consider the mildest symptoms that are common in SARS-CoV-2 infection (for example, runny nose and scratchy throat), resulting in a much less stringent definition of asymptomatic infection than we considered here<sup>33,34</sup>.

Respiratory tract infections are a major public health concern, representing a substantial burden, particularly for young children and the elderly<sup>35,36</sup>. Four strains of seasonal coronaviruses (229E-CoV, NL63-CoV, OC43-CoV and HKU1-CoV) represent 15% to 30% of all respiratory tract infections every year<sup>37</sup>. Notably, previous studies have shown that T cells can cross-react to SARS-CoV-2 and seasonal coronavirus peptides, indicating that long-lasting T cell protective immunity can potentially limit the severity of COVID-19<sup>25</sup>. Moreover, a recent study<sup>28</sup> demonstrated T cell cross-reactivity to SARS-CoV-2 and seasonal coronaviruses for an *HLA-B\*15:01*-restricted immunodominant epitope (NQK-Q8) in individuals who received two doses of the Pfizer-BioNTech BNT162b2 mRNA vaccine. To test the hypothesis that *HLA-B\*15:01* can mediate asymptomatic disease through pre-existing T cell immunity, we analysed immunodominant epitopes in T cells from human PBMCs from pre-pandemic healthy individuals. We observed that T cells from a subset of healthy donors carrying *HLA-B\*15:01* who were never exposed to SARS-CoV-2 were reactive to the SARS-CoV-2 peptide NQK-Q8, and most of the reactive cells displayed a memory phenotype. The sequence identity between SARS-CoV-2 and seasonal coronaviruses peptides, except for a single amino acid substitution, could explain the T cell cross-reactivity. However, a direct demonstration that peptides from SARS-CoV-2 and the seasonal coronaviruses OC43-CoV and HKU1-CoV are stable in the *HLA-B\*15:01* cleft was necessary to further corroborate our hypothesis.

Through our examination of the crystal structures of the *HLA-B\*15:01* molecule in the presence of each peptide, we demonstrated that both NQK-Q8 (SARS-CoV-2) and NQK-A8 (OC43-CoV and HKU1-CoV) spike peptides share a similar ability to stabilize the *HLA-B\*15:01* molecule, and are presented in a similar conformation by *HLA-B\*15:01*, providing the molecular basis for T cell cross-reactivity and pre-existing immunity. This observation is in accordance with previous research in uninfected *HLA-B\*07:02*<sup>+</sup> individuals who are able to recognize the N(105–113) peptide derived from SARS-CoV-2 due to the presence of cross-reactive T cells recognizing the homologous N(105–113) peptide from OC43-CoV and HKU1-CoV<sup>25</sup>. Notably, this T cell cross-reactivity has been associated with less severe COVID-19 disease<sup>38</sup>.

Our data show that both seasonal and pandemic coronavirus-derived NQK peptides can lead to a highly polyfunctional T cell response in the context of *HLA-B\*15:01*, with T cells able to exhibit different effector functions (IFN $\gamma$ , TNF, IL-2, MIP-1 $\beta$ , CD107a). T cell polyfunctionality is critical as it can lead to superior viral-suppressive activity<sup>39,40</sup>; it is linked with high-affinity TCRs that can detect low levels of antigens<sup>39,41</sup>, and it is predictive of protective immunity and vaccine efficacy<sup>42–44</sup>. The high level of polyfunctionality observed for the CD8 $^{+}$  T cells towards the NQK-Q8 peptide in unexposed individuals contrasts with the moderate polyfunctionality observed for the *HLA-B\*07:02*-restricted SARS-CoV-2 N(105–113) peptide (SPRWYFYYL) that also shares a high sequence similarity with the OC43/HKU-1-CoV N(105–113) peptide (LPRWYFYYL)<sup>25</sup>. Although there was some biased TCR gene usage

observed in *HLA-B\*07:02*-N(105–113)-specific TCR repertoire, we did not observe the presence of public TCRs<sup>25</sup>. By contrast, we observed that *HLA-B\*15:01*-NQK-specific TCR repertoire was characterized by the existence of public TCRs. The memory phenotype of the public TCRs in unexposed donors also strongly suggests that they might provide a protective advantage to *HLA-B\*15:01*<sup>+</sup> donors infected by SARS-CoV-2.

The presence of a high level of memory, polyfunctional, high-affinity and public cross-reactive T cells in unexposed donors probably underpins the strong association between the allele *HLA-B\*15:01* and asymptomatic SARS-CoV-2 infection. The presence of cross-reactive public TCRs before infection, observed also after infection or vaccination<sup>28</sup>, could provide a fast and protective immune response in individuals carrying *HLA-B\*15:01*. This characteristic could make *HLA-B\*15:01* a generally more protective allele than *HLA-B\*07:02*, which has been described as potentially limiting the severity of COVID-19 disease<sup>38</sup>. Our results also show the importance of pre-existing immunity<sup>25,28,45,46</sup> giving rise to a memory pool of cross-reactive T cells ready to fight infection<sup>23,37</sup>.

Examination of T cells in patients with asymptomatic SARS-CoV-2 infection has suggested robust T cell responses similar to those with symptomatic disease<sup>47</sup>. Recent studies have shown that SARS-CoV-2-specific memory T cells are enriched at the site of infection compared with in the blood<sup>48</sup>. Thus, the low frequencies of memory T cells that we observed in the blood are probably an under-representation of the resident antigen-specific memory T cells in the respiratory tract that rapidly respond to antigen restimulation at the viral entry sites. Presumably, a pre-existing resident memory T cell population at viral entry sites can lead to a rapid viral clearance before the overt onset of symptoms. Furthermore, the finding that T cells in asymptomatic infection secrete higher quantities of IFN $\gamma$  compared with those in symptomatic patients early in infection<sup>44,47</sup> supports a role for memory T cells at this stage<sup>49</sup>. Although the current literature is mixed regarding cross-reactive CD8 $^{+}$  T cells specific to SARS-CoV-2, this might be explained by HLA specificity<sup>50,51</sup>.

Together, our results strongly support the hypothesis that *HLA-B\*15:01* mediates asymptomatic COVID-19 disease through pre-existing T cell immunity due to previous exposure to HKU1-CoV and OC43-CoV. Notably, the NQK-Q8 peptide is conserved among SARS-CoV-2 variants; moreover, among all *HLA-B15:01*-restricted SARS-CoV-2-derived T cell epitopes reported in the Immune Epitope Database (Supplementary Fig. 8), no other epitope exhibits high sequence identity across common coronaviruses, except for the replicase polyprotein 1ab peptide QLYLGGMSY. However, this last epitope has not been reported in the literature as immunodominant in patients positive for *HLA-B\*15:01* and SARS-CoV-2. On the basis of the limited data available regarding known *HLA-B\*15:01* epitopes in SARS-CoV-2 patients, NQK-Q8 remains the prime candidate peptide underlying any *HLA-B\*15:01*-mediated T cell cross-immunity with seasonal coronaviruses.

One limitation of this study is that all of the testing results and symptoms in our discovery cohort are self-reported. We recognize that this may result in some margin of error in our results. However, we have previously validated this approach by verifying test results in a subset of the participants<sup>52</sup>. Similarly, we did not query some symptoms, notably those related to rash and simple nasal congestion (as opposed to runny nose, which we consider here), and did not consider individuals with only a single symptom report within our two-week window as symptomatic, which may have resulted in some individuals being categorized as asymptomatic when in fact they experienced mild symptoms. However, we incorporated an additional ‘sanity check’ into our classification of asymptomatic disease, where we considered the response to the survey question regarding their reasons to seek testing for SARS-CoV-2 infection. Thus, although our self-report methodology means that we cannot definitively state that our asymptomatic cohort was entirely free

of any symptoms (and in some cases may, rather, be considered mildly symptomatic), we feel confident that our classification of individuals as asymptomatic was generally robust. Importantly, we find a very consistent genetic association across the study and in two independent cohorts where asymptomatic disease was clinician-defined, pointing to a true biological feature.

Another limitation is that our association results are limited to individuals who self-identify as white. While our study cohorts were not well-powered in this regard, we find that our results for *HLA-B\*15:01* appear to trend similarly in Black individuals, although this result is less clear in Asian and Hispanic individuals (Supplementary Table 11). However, owing to the paucity of individuals combined with the lower frequency of this allele in some populations, it is impossible to conclude whether our results for *HLA-B\*15:01* association with asymptomatic disease are applicable in these ancestries. A final limitation is that we tested only four SARS-CoV-2 peptides in our ex vivo analysis. The search for additional candidate peptides will be facilitated as more studies analyse T cell reactivity in patients carrying *HLA-B\*15:01*, similarly to a previous study<sup>28</sup>. However, we identified at least one SARS-CoV-2 peptide previously known to be immunodominant in SARS-CoV-2 infection that was reactive to memory T cells from *HLA-B\*15:01*<sup>+</sup> individuals collected before the pandemic.

In summary, we have demonstrated a strong and significant association of a common *HLA* class I allele, *HLA-B\*15:01*, with asymptomatic infection with SARS-CoV-2. We demonstrated that *HLA-B\*15:01*<sup>+</sup> T cells from pre-pandemic samples were reactive to an immunodominant SARS-CoV-2 peptide that shares high sequence similarity with peptides from seasonal coronaviruses. We provided the molecular basis of T cell cross-reactivity by showing that *HLA-B\*15:01* can stabilize and present peptides from HKU1-CoV and OC43-CoV similarly to the immunodominant peptide from SARS-CoV-2. Moreover, we show that public clonotypes were cross-reactive, polyfunctional and able to recognize both NQK peptides with high affinity. Our results have important implications for understanding early infection and the mechanism underlying early viral clearance and may lay the groundwork for refinement of vaccine development and therapeutic options in early disease.

## Online content

Any methods, additional references, Nature Portfolio reporting summaries, source data, extended data, supplementary information, acknowledgements, peer review information; details of author contributions and competing interests; and statements of data and code availability are available at <https://doi.org/10.1038/s41586-023-06331-x>.

- Meyerowitz, E. A., Richterman, A., Bogoch, I. I., Low, N. & Cevik, M. Towards an accurate and systematic characterisation of persistently asymptomatic infection with SARS-CoV-2. *Lancet Infect. Dis.* **21**, e163–e169 (2020).
- Oran, D. P. & Topol, E. J. Prevalence of asymptomatic SARS-CoV-2 infection. *Ann. Intern. Med.* **173**, M20–M32 (2020).
- Buitrago-Garcia, D. et al. Occurrence and transmission potential of asymptomatic and presymptomatic SARS-CoV-2 infections: a living systematic review and meta-analysis. *PLoS Med.* **17**, e1003346 (2020).
- Ra, S. H. et al. Upper respiratory viral load in asymptomatic individuals and mildly symptomatic patients with SARS-CoV-2 infection. *Thorax* **76**, 61–63 (2021).
- Docherty, A. B. et al. Features of 20133 UK patients in hospital with covid-19 using the ISARIC WHO Clinical Characterisation Protocol: prospective observational cohort study. *Brit. Med. J.* **369**, m1985 (2020).
- The COVID-19 Host Genetics Initiative. The COVID-19 Host Genetics Initiative, a global initiative to elucidate the role of host genetic factors in susceptibility and severity of the SARS-CoV-2 virus pandemic. *Eur. J. Hum. Genet.* **28**, 715–718 (2020).
- The Severe Covid-19 GWAS Group. Genomewide association study of severe Covid-19 with respiratory failure. *New Engl. J. Med.* **383**, 1522–1534 (2020).
- Pairo-Castineira, E. et al. Genetic mechanisms of critical illness in COVID-19. *Nature* **591**, 92–98 (2021).
- Martin, M. P. & Carrington, M. Immunogenetics of HIV disease. *Immunol. Rev.* **254**, 245–264 (2013).
- Blackwell, J. M., Jamieson, S. E. & Burgner, D. HLA and infectious diseases. *Clin. Microbiol. Rev.* **22**, 370–385 (2009).
- Lin, M. et al. Association of HLA class I with severe acute respiratory syndrome coronavirus infection. *BMC Med. Genet.* **4**, 9–7 (2003).
- Chen, Y.-M. A. et al. Epidemiological and genetic correlates of severe acute respiratory syndrome coronavirus infection in the hospital with the highest nosocomial infection rate in Taiwan in 2003. *J. Clin. Microbiol.* **44**, 359–365 (2006).
- Ng, M. H. L. et al. Association of human-leukocyte-antigen class I (B\*0703) and class II (DRB1\*0301) genotypes with susceptibility and resistance to the development of severe acute respiratory syndrome. *J. Infect. Dis.* **190**, 515–518 (2004).
- Ahmed, S. F., Quadeer, A. A. & McKay, M. R. Preliminary identification of potential vaccine targets for the COVID-19 coronavirus (SARS-CoV-2) based on SARS-CoV immunological studies. *Viruses* **12**, 254 (2020).
- Lee, C. H. & Koohy, H. In silico identification of vaccine targets for 2019-nCoV. *F1000Research* **9**, 145 (2020).
- Nguyen, A. et al. Human leukocyte antigen susceptibility map for severe acute respiratory syndrome coronavirus 2. *J. Virol.* **94**, e00510-20 (2020).
- Enayatkhani, M. et al. Reverse vaccinology approach to design a novel multi-epitope vaccine candidate against COVID-19: an in silico study. *J. Biomol. Struct. Dyn.* **39**, 2857–2872 (2020).
- Augusto, D. G. & Hollenbach, J. A. HLA variation and antigen presentation in COVID-19 and SARS-CoV-2 infection. *Curr. Opin. Immunol.* **76**, 102178 (2022).
- Aguilar, V. R. C. et al. An immunogenetic view of COVID-19. *Genet. Mol. Biol.* **44**, e20210036 (2021).
- Hollenbach, J. A. & Srivastava, A. The immunogenetics of COVID-19. *Immunogenetics* <https://doi.org/10.1007/s00251-022-01284-3> (2022).
- COVID-19 Host Genetics Initiative. Mapping the human genetic architecture of COVID-19. *Nature* **600**, 472–477 (2021).
- Langton, D. J. et al. The influence of HLA genotype on the severity of COVID-19 infection. *HLA* **98**, 14–22 (2021).
- Davis, M. M., Altman, J. D. & Newell, E. W. Interrogating the repertoire: broadening the scope of peptide–MHC multimer analysis. *Nat. Rev. Immunol.* **11**, 551–558 (2011).
- Francis, J. M. et al. Allelic variation in class I HLA determines CD8<sup>+</sup> T cell repertoire shape and cross-reactive memory responses to SARS-CoV-2. *Sci. Immunol.* **7**, eabk3070 (2021).
- Lineburg, K. E. et al. CD8<sup>+</sup> T cells specific for an immunodominant SARS-CoV-2 nucleocapsid epitope cross-react with selective seasonal coronaviruses. *Immunity* **54**, 1055–1065 (2021).
- Saini, S. K. et al. SARS-CoV-2 genome-wide T cell epitope mapping reveals immunodominance and substantial CD8<sup>+</sup> T cell activation in COVID-19 patients. *Sci. Immunol.* **6**, eabf7550 (2021).
- Gangaev, A. et al. Identification and characterization of a SARS-CoV-2 specific CD8<sup>+</sup> T cell response with immunodominant features. *Nat. Commun.* **12**, 2593 (2021).
- Minervina, A. A. et al. SARS-CoV-2 antigen exposure history shapes phenotypes and specificity of memory CD8<sup>+</sup> T cells. *Nat. Immunol.* **23**, 781–790 (2022).
- Gras, S., Kjer-Nielsen, L., Burrows, S. R., McCluskey, J. & Rossjohn, J. T-cell receptor bias and immunity. *Curr. Opin. Immunol.* **20**, 119–125 (2008).
- Nguyen, A. T., Szeto, C. & Gras, S. The pockets guide to HLA class I molecules. *Biochem. Soc. Trans.* **49**, 2319–2331 (2021).
- Grageret, L., Madabouly, A., Freeman, J. & Maiers, M. Six-locus high resolution HLA haplotype frequencies derived from mixed-resolution DNA typing for the entire US donor registry. *Hum. Immunol.* **74**, 1313–1320 (2013).
- Astbury, S. et al. HLA-DR polymorphism in SARS-CoV-2 infection and susceptibility to symptomatic COVID-19. *Immunology* **166**, 68–77 (2022).
- Nguyen, A., Yusufali, T., Hollenbach, J. A., Nellore, A. & Thompson, R. F. Minimal observed impact of HLA genotype on hospitalization and severity of SARS-CoV-2 infection. *HLA* **99**, 607–613 (2022).
- Schetelij, J. et al. Individual HLA-A, -B, -C, and -DRB1 genotypes are no major factors which determine COVID-19 severity. *Front. Immunol.* **12**, 698193 (2021).
- Williams, B. G., Gouws, E., Boschi-Pinto, C., Bryce, J. & Dye, C. Estimates of world-wide distribution of child deaths from acute respiratory infections. *Lancet Infect. Dis.* **2**, 25–32 (2002).
- Ge, X., Guo, Y., Cheng, J., Hu, R. & Feng, X. Epidemiology and seasonality of respiratory viruses detected from children with respiratory tract infections in Wuxi, East China. *Med. Sci. Monit.* **24**, 1856–1862 (2018).
- Guthmiller, J. J. & Wilson, P. C. Remembering seasonal coronaviruses. *Science* **370**, 1272–1273 (2020).
- Peng, Y. et al. An immunodominant NP105–113-B\*07:02 cytotoxic T cell response controls viral replication and is associated with less severe COVID-19 disease. *Nat. Immunol.* **23**, 50–61 (2022).
- Galperin, M. et al. CD4<sup>+</sup> T cell-mediated HLA class II cross-restriction in HIV controllers. *Sci. Immunol.* **3**, eaat0687 (2018).
- Almeida, J. R. et al. Antigen sensitivity is a major determinant of CD8<sup>+</sup> T-cell polyfunctionality and HIV-suppressive activity. *Blood* **113**, 6351–6360 (2009).
- Tan, M. P. et al. T cell receptor binding affinity governs the functional profile of cancer-specific CD8<sup>+</sup> T cells. *Clin. Exp. Immunol.* **180**, 255–270 (2015).
- Makedonas, G. & Betts, M. R. Polyfunctional analysis of human T cell responses: importance in vaccine immunogenicity and natural infection. *Springer Semin. Immunopathol.* **28**, 209–219 (2006).
- Duvall, M. G. et al. Polyfunctional T cell responses are a hallmark of HIV-2 infection. *Eur. J. Immunol.* **38**, 350–363 (2008).
- Sekine, T. et al. Robust T cell immunity in convalescent individuals with asymptomatic or mild COVID-19. *Cell* **183**, 158–168 (2020).
- Rivino, L. & Wooldridge, L. Ready and waiting to go. *eLife* **12**, e85080 (2023).
- Pothast, C. R. et al. SARS-CoV-2-specific CD4<sup>+</sup> and CD8<sup>+</sup> T cell responses can originate from cross-reactive CMV-specific T cells. *eLife* **11**, e82050 (2022).
- Bert, N. L. et al. Highly functional virus-specific cellular immune response in asymptomatic SARS-CoV-2 infection. *J. Exp. Med.* **218**, e20202617 (2021).
- Cheon, S. et al. Immune signatures underlying post-acute COVID-19 lung sequelae. *Sci. Immunol.* **6**, eabk1741 (2021).

49. Kambayashi, T., Assarsson, E., Lukacher, A. E., Ljunggren, H.-G. & Jensen, P. E. Memory CD8<sup>+</sup> T cells provide an early source of IFN- $\gamma$ . *J. Immunol.* **170**, 2399–2408 (2003).

50. Ferretti, A. P. et al. Unbiased screens show CD8<sup>+</sup> T cells of COVID-19 patients recognize shared epitopes in SARS-CoV-2 that largely reside outside the spike protein. *Immunity* **53**, 1095–1107 (2020).

51. Lipsitch, M., Grad, Y. H., Sette, A. & Crotty, S. Cross-reactive memory T cells and herd immunity to SARS-CoV-2. *Nat. Rev. Immunol.* **20**, 709–713 (2020).

52. Aung, S. et al. Characteristics and behaviors associated with prevalent SARS-CoV-2 infection. *Int. J. Gen. Med.* **14**, 1063–1067 (2021).

**Publisher's note** Springer Nature remains neutral with regard to jurisdictional claims in published maps and institutional affiliations.



**Open Access** This article is licensed under a Creative Commons Attribution 4.0 International License, which permits use, sharing, adaptation, distribution and reproduction in any medium or format, as long as you give appropriate credit to the original author(s) and the source, provide a link to the Creative Commons licence, and indicate if changes were made. The images or other third party material in this article are included in the article's Creative Commons licence, unless indicated otherwise in a credit line to the material. If material is not included in the article's Creative Commons licence and your intended use is not permitted by statutory regulation or exceeds the permitted use, you will need to obtain permission directly from the copyright holder. To view a copy of this licence, visit <http://creativecommons.org/licenses/by/4.0/>.

© The Author(s) 2023

<sup>1</sup>Weill Institute for Neurosciences, Department of Neurology, University of California, San Francisco, CA, USA. <sup>2</sup>Department of Biological Sciences, The University of North Carolina at Charlotte, Charlotte, NC, USA. <sup>3</sup>Programa de Pós-Graduação em Genética, Universidade Federal do Paraná, Curitiba, Brazil. <sup>4</sup>Department of Biochemistry and Chemistry, La Trobe Institute for Molecular Science, La Trobe University, Bundoora, Victoria, Australia. <sup>5</sup>Department of Biochemistry and Molecular Biology, Biomedicine Discovery Institute, Monash University, Clayton, Victoria, Australia. <sup>6</sup>Division of Cardiology, Department of Medicine, University of California, San Francisco, CA, USA. <sup>7</sup>Division of HIV, Infectious Diseases and Global Medicine, Department of Medicine, University of California, San Francisco, CA, USA. <sup>8</sup>Department of Laboratory Medicine, University of California, San Francisco, CA, USA. <sup>9</sup>Clinical and Translational Science Institute, University of Utah, Salt Lake City, UT, USA. <sup>10</sup>Division of Experimental Medicine, Department of Medicine, University of California, San Francisco, CA, USA. <sup>11</sup>Department of Medicine, University of California, San Francisco, CA, USA. <sup>12</sup>Department of Epidemiology and Biostatistics, University of California, San Francisco, CA, USA. <sup>13</sup>F.J. Proctor Foundation, University of California, San Francisco, CA, USA. <sup>14</sup>CIBMTR (Center for International Blood and Marrow Transplant Research), National Marrow Donor Program/Be The Match, Minneapolis, MN, USA. <sup>15</sup>ExplantLab, Newcastle-upon-Tyne, UK. <sup>16</sup>QIMR Berghofer Centre for Immunotherapy and Vaccine Development Brisbane, QIMR Berghofer Medical Research Institute, Brisbane, Queensland, Australia. <sup>17</sup>Division of General Internal Medicine, University of California, San Francisco, CA, USA. <sup>18</sup>These authors contributed equally: Danillo G. Augusto, Lawton D. Mardolo, Demetra S. M. Chatzileontiadou. <sup>19</sup>These authors jointly supervised this work: Stephanie Gras, Jill A. Hollenbach. <sup>20</sup>e-mail: jill.hollenbach@ucsf.edu

# Article

## Methods

### Data collection for the discovery (Citizen Science) cohort

The study participants were volunteer bone marrow donors with valid e-mail addresses on file with the National Marrow Donor Program (NMDP) who were invited to participate in the study through an e-mail outreach campaign that began in July 2020. All individuals had within the NMDP database a pre-existing record for high-resolution *HLA* genotyping, typically for five loci (*HLA-A*, *-B*, *-C*, *-DRB1* and *-DQB1*)<sup>31</sup>. Participants who opt in to the study are required to download a smartphone app and participate in the COVID-19 Citizen Science Study (launched using the Eureka Digital Research Platform; <https://eureka.app.link/covid19>) or, as of January 2021, participate through the website (<https://covid19.eurekaplatform.org/>). Once enrolled, the participants are asked to complete an initial 10 to 15 min survey about baseline demographics, their health history and daily habits. Follow-up daily questions specific to symptoms, weekly questions regarding testing and monthly questions regarding hospitalization for COVID-19 are delivered by push notification or text message on an ongoing basis and require 5 to 15 min per week. As of 30 April 2021, we enrolled 29,947 individuals, of whom 21,893 have completed their baseline survey (Supplementary Table 12). Participation in the UCSF Citizen Science study and linking to NMDP *HLA* data were approved by the Institutional Review Board for the University of California, San Francisco (IRB 17-21879 and IRB 20-30850, respectively). All of the participants provided written informed consent agreeing to research and publication of research results.

Within the mobile application, the survey respondents are asked during their initial baseline survey whether they have ever been tested for active infection and report the result (positive, negative, do not know) and the approximate number of weeks since the test. Thereafter, each week respondents are asked whether they were tested in the previous week, and to report the result. We considered anybody reporting a positive test for active infection as having been infected with SARS-CoV-2. Our cohort consisted of individuals reporting a positive test for virus up to 30 April 2021 before the implementation of widespread vaccination for the virus. We restricted the analysis to individuals who had self-identified as 'white' only due to insufficient numbers for analysis in the other groups (Supplementary Tables 13 and 14), allowing an analysis of 1,428 individuals. The inclusion criteria are provided in Supplementary Fig. 9.

Symptoms are self-reported at the baseline and in daily surveys. Within the baseline survey, the respondents are asked to report whether they had any of a list of symptoms (Supplementary Table 15) for 3 days or longer at any time since February 2020. These same symptoms are queried in each daily survey, where respondents are asked whether they experienced each symptom within the previous 24 h. Among those individuals, we considered those as asymptomatic who reported having had a positive test for active virus at the baseline, with a time since the test of longer than 2 weeks or who did not specify test dates, and who reported "None of the above" for all symptoms in the baseline survey. We also considered daily symptom reports for the 2 weeks after the baseline for respondents who reported a positive test for active infection at the baseline as having occurred within the previous 2 weeks. In these cases, we considered individuals asymptomatic if, in addition to reporting no symptoms at baseline, they did not report any single symptom two or more times within this time period. For individuals who did not report a positive test for active infection at the baseline, but subsequently reported a positive test on a weekly survey, we used the same criteria considering daily symptom reports for the period 2 weeks before and 2 weeks after the positive test report (Supplementary Fig. 10). To further confirm a lack of symptoms, we also considered the survey question "Why was the test for active COVID-19 infection (virus) performed?" (Supplementary Table 16). Individuals who otherwise did not report symptoms, but responded "I had symptoms concerning for COVID-19 infection" were categorized as symptomatic.

### The CHIRP and LIINC (replication) cohorts

The study participants were enrolled in two UCSF-based prospective longitudinal cohorts: the CHIRP study and the LIINC study. The participants were identified through local clinical systems (UCSF Moffitt Hospital, San Francisco General Hospital, Kaiser, California Pacific Medical Center) as well as the San Francisco Department of Public Health. After confirmation of SARS-CoV-2 test results or exposure to determine eligibility, the participants were asked to sign a consent form, complete a baseline visit and schedule follow-up in-person visits. The CHIRP study included volunteers with positive PCR test documentation and/or symptom onset within the preceding 21 days. Asymptomatic disease was defined as having a confirmed positive PCR test with lack of any symptoms ("Did you have or are you still having any symptoms that you think are because of COVID-19?") at the baseline and follow-up visits. A total of five longitudinal samples were collected from participants with acute SARS-CoV-2 infection. The first sample was collected <31 days of symptom onset or <31 days from exposure to SARS-CoV-2 as a week 0 baseline visit. The remaining samples were collected at weeks 1, 3, 10 and 24. At each CHIRP visit, blood and nasopharyngeal swabs were collected. Optional sample collection included sputum, saliva, stool and urine. The LIINC study enrolled participants with previous SARS-CoV-2 infection confirmed on clinical nucleic acid amplification testing between 14 and 90 days after initial symptom onset. After written informed consent, clinical data and biospecimens were collected monthly for up to 4 months after initial symptom onset and then every 4 months thereafter. Biospecimens including blood and saliva were collected at each visit. CHIRP and LIINC used a harmonized set of case report forms to collect clinical data about demographics, medical history, the COVID-19 illness and post-acute symptoms. Clinical measurements collected during in-person CHIRP visits included complete blood count with differential, comprehensive metabolic panel, erythrocyte sedimentation rate, high-sensitivity C-reactive protein, d-dimer, lactate dehydrogenase and ferritin. All of the participants provided written informed consent agreeing to research and publication of research results, and the CHIRP and LIINC studies were approved by the Institutional Review Board for the University of California, San Francisco (IRB 20-30588 and 20-30479, respectively).

### HLA genotyping in the CHIRP/LIINC cohort

A total of 100 ng of high-quality DNA was fragmented using the Library Preparation Enzymatic Fragmentation Kit 2.0 (Twist Bioscience). Subsequently, the ends of the fragmented DNA were repaired, poly(A) tails were added and ligated through PCR to Illumina-compatible dual index adapters that were uniquely barcoded. After ligation, fragments were purified with a 0.8× ratio AMPure XP magnetic beads (Beckman Coulter), followed by dual-size selection (0.42× and 0.15× ratios) to select libraries of approximately 800 bp. Finally, libraries were amplified and purified with magnetic beads.

After fluorometric quantification, 30 ng of each sample was precisely pooled using ultrasonic acoustic energy, and the targeted capture was performed using the Twist Target Enrichment kit (Twist Bioscience). In brief, the volumes were reduced using magnetic beads, and the DNA libraries were bound to 1,394 biotinylated probes specific to the *HLA* region, covering all exons, introns and regulatory regions of *HLA-A*, *HLA-B*, *HLA-C*, *HLA-DRB1*, *HLA-DRA*, *HLA-DQB1*, *HLA-DQA1*, *HLA-DPB1* and *HLA-DPA1*. Fragments targeted by the probes were captured using Streptavidin magnetic beads and then amplified and purified. Enriched libraries were analysed using the BioAnalyzer (Agilent) and quantified by droplet digital PCR. Finally, enriched libraries were sequenced using the NovaSeq platform (Illumina) with a paired-end 150 bp sequencing protocol. After sequencing, data were analysed using HLA Explorer v.1.4 (Omixon) and AlloSeq Tx V471 (CareDx).

## UK cohort reanalysis

We reanalysed the primary data from a previous study<sup>22</sup> that analysed HLA class I and class II genes in 147 individuals of European ancestry with known SARS-CoV-2 infection and a range of symptoms and 69 asymptomatic hospital workers. In the initial publication, *HLA-B\*15:01* was not directly tested for association with asymptomatic disease course. *HLA* genotyping methods, allele frequencies, demographics and clinical outcomes are as previously described.

## HLA association analysis

In our discovery cohort, we examined the association of five *HLA* loci (*HLA-A*, *-B*, *-C*, *-DRB1* and *-DQB1*) with asymptomatic versus symptomatic infection. Data analysis included the first two fields of the allele name as described in the HLA nomenclature, representing the complete molecule at polypeptide sequence resolution.

Initial testing for *HLA* associations was performed using the R package BIGDAWG<sup>53</sup>, which handles multiallelic *HLA* data to test for association at the haplotype, locus, allele and amino acid levels. We next used a generalized linear model using *glm* in the R (v.4.3) base package to consider the relevant covariates, including any reported comorbidities, sex and age, for alleles that were initially found to be associated with asymptomatic infection after correction for multiple testing. We corrected *P* values using the Bonferroni method<sup>54</sup> for the number of alleles tested at *HLA-A*, *-B* and *-DRB1*, which accounts for the strong linkage disequilibrium between some of the loci tested. For the replication cohorts, we tested only the allele of interest, using the generalized linear model framework as described. Meta-analysis of the results in our three cohorts was performed in R using the common effect model with the meta package (v.6.2-1)<sup>55</sup>.

## Peptide synthesis

The four SARS-CoV-2 peptides (Fig. 1a–c and Supplementary Table 17) were synthesized by in vitro transcription and translation of oligonucleotides encoding each peptide using the PURExpress in vitro protein synthesis kit (New England BioLabs) as previously described<sup>56</sup>. Peptides NQK-Q8 (NQKLIANQF) and NKQ-A8 (NQKLIANAF) (used in Figs. 1d and 2–4) were synthesized using the fluoren-9-ylmethoxycarbonyl (Fmoc) method of solid-phase peptide synthesis. The process was performed using the Biotage Initiator+ Alstra automated peptide synthesizer and Wang resin (100–200 mesh, 1.24 mmol g<sup>-1</sup>), which was swollen in dimethylformamide (DMF) for 2 h before use. The Fmoc-amino acids and HCTU/HOBt/DIPEA (4 eq.) dissolved in DMF were then added sequentially to the resin and the coupling reactions were carried out with microwave heating at 60 °C for 20 min. The Fmoc protecting groups were removed using piperidine (20% in DMF) at room temperature for 20 min. The peptides were cleaved from the resin using a mixture of 95% trifluoroacetic acid (TFA) and 5% triisopropylsilane (TIPS) for 3 h. After evaporation of the TFA/TIPS mixture and precipitation with diethyl ether, the crude peptides were purified using reversed-phase high-performance liquid chromatography (HPLC) on the Shimadzu HPLC system fitted with two Shimadzu LC-20AD pumps, a SIL-20AHT autosampler, SPD-M20A photodiode array detector and a FRC-10A fraction collector and an Onyx Monolithic C18, 100 × 10 mm semipreparative column with a solvent system consisting of 0.1% TFA in water and acetonitrile over 30 min. The purified peptides were lyophilized and stored at -20 °C. The purity was confirmed to be >95% in each case by analytical HPLC and the structures were confirmed using high-resolution electrospray ionization mass spectrometry (Supplementary Fig. 11).

## PBMCs

A total of 20 unexposed and 1 triple-vaccinated (VAC62) donors were recruited; all details are provided in Supplementary Table 18. PBMCs were separated from whole blood or buffy coats using density-gradient

centrifugation. PBMCs were used fresh or were cryogenically stored until use. HLA-genotyped PBMCs from the USA were stored in the National Marrow Donor Program (NMDP)/Be The Match Research Sample Repository (ClinicalTrials.gov protocol NCT04920474) that had been collected from healthy donors before the start of the COVID-19 pandemic. All individuals consented to research and publication of research results and had been previously genotyped for *HLA* class I and class II. Ethics approval to undertake the research was obtained from the QIMR Berghofer Medical Research Institute Human Research Ethics Committee (P2282) and La Trobe University Human Research Ethics Committee (HEC21097). The *HLA* genotyping was performed by AlloSeq Tx17 (CareDx Pty) using AllType NGS high-resolution genotyping on the IonTorrent NGS platform.

## TAME

Each peptide was loaded on biotinylated *HLA-B\*15:01* (either custom-made or purchased from easYmers immunAware) according to the manufacturer's instructions.

For the combinatorial tetramer staining that included all four SARS-CoV-2 peptides (Supplementary Table 17) related to Fig. 1a–c, peptide-loaded *HLA-B\*15:01* tetramers were generated using Streptavidin conjugated to PE, APC, PE-CF594 or BV421 according to the manufacturer's instructions. D-Biotin (500 μM) was subsequently added to each peptide-loaded tetramer and tetramers were pooled just before cell staining. Combinatorial tetramer staining was used to identify each epitope by unique combinations of dual fluorophores where at least one of the fluorophores contained PE (Supplementary Table 17). The frequencies of antigen-specific T cells were calculated as previously described<sup>57</sup>. In brief, an aliquot of PBMCs was used for cell surface staining and counting using 123count eBeads (Invitrogen). The remaining PBMCs were stained with the indicated tetramer pools and enriched using anti-PE magnetic microbeads (Miltenyi) over a magnetic column, cell-surface stained and counted as for pre-enrichment. CD8<sup>+</sup> T cells were identified by gating live singlet CD8<sup>+</sup> lymphocytes that were negative for CD4, CD14, CD16 and CD19 (Supplementary Fig. 2 and Supplementary Table 19). A stringent tetramer gating strategy was used whereby CD8<sup>+</sup> T cells labelled with only two fluorophores were considered antigen specific. The memory status of tetramer-positive CD8<sup>+</sup> T cells was determined by lack of CCR7 and CD45RA co-expression. Given the low numbers of cells available from donors, only tetramer<sup>+</sup>CD8<sup>+</sup> T cells with frequencies of greater than 1 × 10<sup>-4</sup> per total CD8<sup>+</sup> T cells were considered to be positive.

For the tetramer staining that included only the NQK-Q8 and NKQ-A8 peptides (related to Figs. 1d and 2 and Extended Data Fig. 1), peptide-loaded *HLA-B\*15:01* tetramers were generated using Streptavidin conjugated to phycoerythrin (PE). Tetramer-stained cells were enriched using anti-PE antibody-coated immunomagnetic beads on LS columns (Miltenyi Biotech) according to manufacturer instructions. After enrichment, cells were stained with an antibody panel including anti-CD3-BV480 (dilution 1:100), anti-CD8-PerCP-Cy5.5 (1:50), anti-CD4-BV650 (1:100), anti-CD14-APC-H7 (1:200), anti-CD19-APC-H7 (1:100), anti-CD45RA-FITC (1:100), anti-CD27-APC (1:100), anti-CCR7-PE-Cy7 (1:50), anti-CD95-BV421 (1:50), anti-PD1-BV605 (1:100) (all BD Biosciences) and Live/Dead Fixable Near-IR Dead Cell Stain (1:1,000) (Life Technologies) (Supplementary Fig. 4). Cells were resuspended in MACS buffer (PBS, 0.5% BSA, 2 mM EDTA) and were directly single-cell index sorted into PCR plates (Eppendorf) using the BD Aria Fusion system.

## Generation of peptide-specific CD8<sup>+</sup> T cell lines

CD8<sup>+</sup> T cell lines were generated as previously described<sup>25,58</sup>. In brief, PBMCs were incubated with 1 μM of individual peptide (NQK-Q8 or NKQ-A8) and cultured for 10–14 days in RPMI-1640 supplemented with 2 mM MEM non-essential amino acid solution (Sigma-Aldrich), 100 mM HEPES (Sigma-Aldrich), 2 mM L-glutamine (Sigma-Aldrich),

penicillin–streptomycin (Life Technologies), 50 mM 2-ME (Sigma-Aldrich) and 10% heat-inactivated fetal bovine serum (Bovogen). The cultures were supplemented with 10 IU IL-22–3 times weekly. CD8<sup>+</sup> T cell lines were used fresh for subsequent analysis. For the double tetramer staining experiments  $0.5 \times 10^6$  cells from the CD8<sup>+</sup> T cell lines were stained with a single PE-conjugated tetramer (HLA-B\*15:01-NQK-Q8 or HLA-B\*15:01-NQK-A8) or double stained with both tetramers (PE-conjugated NQK-A8 and APC-conjugated NQK-Q8 tetramer) for 1 h at room temperature. Cells were washed and surface-stained with anti-CD3-BV480 (dilution 1:100), anti-CD8-PerCP-Cy5.5 (1:50), anti-CD4-BV650 (1:100), anti-CD14-APCH7 (1:200) and anti-CD19-APCH7 (1:100) antibodies (all BD Biosciences) and Live/Dead Fixable Near-IR Dead Cell Stain (Life Technologies). Cells were single-cell sorted into PCR plates (Eppendorf) using the BD Aria Fusion system.

### Intracellular cytokine assay

CD8<sup>+</sup> T cell lines were stimulated with 1  $\mu$ M of the cognate or the homologous peptide and were incubated for 4–5 h in the presence of GolgiPlug, GolgiStop and anti-CD107a-FITC (dilution 1:100) (all BD Biosciences). After stimulation, cells were surface stained for 30 min with anti-CD3-BV480 (1:100), anti-CD8-PerCP-Cy5.5 (1:50) and anti-CD4-BV650 (1:100) antibodies (all BD Biosciences) and Live/Dead Fixable Near-IR Dead Cell Stain (Life Technologies). Cells were fixed and permeabilized using BD Cytofix/Cytoperm solution (BD Biosciences) and then intracellularly stained with anti-IFN- $\gamma$ -BV421 (1:100), anti-TNF-PE-Cy7 (1:100), anti-IL2-PE (1:100) and anti-MIP-1 $\beta$ -APC (1:100) antibodies (all BD Biosciences) for a further 30 min. Cells were acquired on the BD FACSymphony A3 system using the FACSDiva software (v.9.0.). Post-acquisition analysis was performed using FlowJo software (v.10). Cytokine detection levels identified in the no-peptide control condition were subtracted from the corresponding test conditions in all summary graphs to account for non-specific, spontaneous cytokine production.

### Single-cell multiplex PCR

Single-cell multiplex PCR was performed as previously described<sup>59</sup>. In brief, cDNA was generated using the VIVO cDNA synthesis kit (Invitrogen) at 1/20 of the manufacturer's recommendations with 0.1% Triton X-100. Nested PCR comprising 40  $\alpha$ - and 27  $\beta$ -chains was subsequently undertaken. PCR products were purified using ExoSAP (GE Healthcare) and were sequenced at AGRF. Sequences were analysed using FinchTV (Geospiza v.1.5.0) and IMGT software<sup>60</sup>. CDR3 sequences shown are all productive (no stop codons)<sup>61</sup>.

### SPR analysis

SPR experiments were conducted at 25 °C on the BIAcore T200 instrument in 10 mM Tris-HCl, pH 8.0 (Fisher Bioreagents), 150 mM NaCl (Merck), 0.005% surfactant P20 (Cytiva) and 0.5% BSA (Sigma-Aldrich). Streptavidin chips were used to bind biotinylated HLA-B\*15:01-NQK complexes (coupled at ~4,000 response units). The first flow cell was loaded with H2D<sup>b</sup>-PA (negative control). The experiments were conducted with ten serial dilutions of the TCRs starting at 100 or 150  $\mu$ M. All of the experiments were conducted in duplicate twice ( $n = 2$  independent experiment). BIAevaluation (v.3.1) and GraphPad Prism 9 (v.9.3) were used for data analysis reported in Supplementary Table 10.

### Analysis of the TCR clonotypic repertoire

TRA and TRB sequences were analysed using the software suite from the International ImMunoGeneTics (IMGT) Information System<sup>62</sup>. The V(D)J gene nomenclature used is that of the IMGT database ([www.imgt.org](http://www.imgt.org)). Motifs enriched were identified using the MEME suite motif discovery software (v.5.5.2.)<sup>63</sup>. The MEME software chooses the width and number of occurrences of each motif automatically to minimize the  $E$ -value of the motif. Motifs were searched in discriminative mode and were represented as sequence logos, where the relative sizes of the

letters indicate their frequencies in the sequence set, and the total height of the letters represents the information content of the position, in bits.

### Statistical analysis

GraphPad Prism 9 (v.9.3) was used to perform statistical analysis. Statistical comparisons between groups were determined using one-way or two-way analysis of variance with correction for multiple comparisons.  $P < 0.05$  was considered to be significant.

### Protein expression, refold and purification

HLA-B\*15:01 heavy chain,  $\beta$ 2-microglobulin and TCR  $\alpha$ - and  $\beta$ -chains were expressed in *BL21 Escherichia coli* cells as inclusion bodies. HLA-B\*15:01 was refolded and purified as described previously<sup>61</sup>. In brief, soluble HLA-B\*15:01-NQK-Q8 or -A8 complexes were produced by refolding inclusion bodies at the following amounts: 30 mg of heavy chain, 10 mg of  $\beta$ 2-microglobulin and 5 mg of the peptide into 200 ml of buffer (100 mM Tris-HCl pH 8.0 (Fisher Bioreagents), 400 mM L-arginine (Sigma-Aldrich), 500  $\mu$ M glutathione oxidized (Goldbio), 5 mM glutathione reduced (Goldbio), 20 mM EDTA (Sigma-Aldrich)). The *TRBV7-2* gene has four alleles (*TRBV7-2\*01* and *TRBV7-2\*02/03/04*), changing the Ser45 to Arg45 upstream of the CDR2 $\beta$  loop and Gly84 to Glu84 of the HV4 loop<sup>64</sup> that could impact pHLA recognition. From the TCR sequencing results, we could not differentiate the alleles. As *TRBV7-2\*02/03/04* are similar at the protein level, we produced the TCRs with either *TRBV7-2\*01* or *TRBV7-2\*02*. The SPR results show that the polymorphism within the  $\beta$ -chain did not impact the pHLA recognition (Extended Data Figs. 7 and 8 and Supplementary Table 10). TCRs were refolded by mixing 100 mg of the  $\alpha$ -chain and 50 mg of the  $\beta$ -chain in 400 ml of the same buffer containing 5 M urea (Sigma-Aldrich). The refold mixtures were dialysed into 10 mM Tris-HCl pH 8.0 (Fisher Bioreagents). The HLA-B\*15:01-NQK complexes and the TCRs were purified using anion-exchange chromatography (DEAE and HiTrap Q, both GE Healthcare).

### DSF analysis

Thermal stability assays were performed by DSF using the ViiA 7 real-time PCR system (Thermo Fisher Scientific), in which the HLA-B\*15:01-YFP complex was heated from 25 to 95 °C at a rate of 1 °C min<sup>-1</sup> in 0.5 °C steps. The excitation and emission channels were set to the TAMRA reporter (x3m3 filter) with excitation of ~550 nm and detection at ~587 nm. The experiment was performed at two concentrations of pHLA (5  $\mu$ M and 10  $\mu$ M) in duplicates. Each sample was dialysed in 10 mM Tris-HCl pH 8.0 (Fisher Bioreagents), 150 mM NaCl (Merck) and contained a final concentration of 10× SYPRO Orange Dye (Invitrogen). Fluorescence intensity data were normalized and plotted using GraphPad Prism 9 (v.9.3). The  $T_m$  value for a pHLA is equal to the temperature at which 50% of maximum fluorescence intensity is reached, which is equal to approximately 50% of unfolded protein and is summarized in Supplementary Table 9.

### Crystallization and structure determination

Crystals of HLA-B\*15:01–peptide complexes were grown by hanging-drop vapour diffusion at 20 °C. The protein:reservoir drop ratio was 1:1, at a concentration of 3 mg ml<sup>-1</sup> in 10 mM Tris-HCl pH 8 (Fisher Bioreagents), 150 mM NaCl (Merck). Crystals of HLA-B\*15:01-NQK-Q8 were grown in 0.2 M sodium formate pH 7.0 and 20% (w/v) polyethylene glycol 3350; and, for HLA-B\*15:01-NQK-A8, in 20% (w/v) polyethylene glycol 3350 and 2% (v/v) ethylene glycol. Protein crystals were soaked in a cryoprotectant solution containing mother liquor solution with 20% (v/v) ethylene glycol and then flash-frozen in liquid nitrogen. The data were collected on the MX2 beamline at the Australian Synchrotron, part of ANSTO, Australia<sup>65</sup>. The data were processed using XDS<sup>66</sup> and the structures were determined by molecular replacement using the PHASER program (v.2.8.3)<sup>67</sup> from the CCP4 suite<sup>68</sup> with a model

of HLA-B\*15:01 without the peptide (derived from Protein Data Bank (PDB) 5TXS)<sup>69</sup>. Manual model building was conducted using COOT<sup>70</sup> followed by refinement with BUSTER<sup>71</sup> and PHENIX (v.1.20.1-4487)<sup>72</sup>. The final models have been validated and deposited using the wwPDB OneDep System and the final refinement statistics and PDB codes are summarized in Extended Data Table 2. All molecular graphic representations were created using PyMOL (v.2.5).

## Reporting summary

Further information on research design is available in the Nature Portfolio Reporting Summary linked to this article.

## Data availability

All HLA and phenotypic data for the Citizen Science and CHIRP/LIINC and UK cohorts are available in the online public database (<http://www.hiacovid19.org/database/>; Project 3 Hollenbach and Project 6 Langton). The crystallography structures are available at the PDB under accession codes 8ELG and 8ELH for HLA-B\*15:01–NQK-A8 and HLA-B\*15:01–Q8, respectively.

53. Pappas, D. J., Marin, W., Hollenbach, J. A. & Mack, S. J. Bridging ImmunoGenomic Data Analysis Workflow Gaps (BIGDAWG): an integrated case-control analysis pipeline. *Hum. Immunol.* **77**, 283–287 (2016).
54. Bland, J. M. & Altman, D. G. Multiple significance tests: the Bonferroni method. *Brit. Med. J.* **310**, 170 (1995).
55. Schwarzer, G., Carpenter, J. R. & Rücker, G. *Meta-Analysis with R* <https://doi.org/10.1007/978-3-319-21416-0> (Springer, 2015).
56. Ma, K.-Y. et al. High-throughput and high-dimensional single-cell analysis of antigen-specific CD8<sup>+</sup> T cells. *Nat. Immunol.* **22**, 1590–1598 (2021).
57. Sabatino, J. J. S. Jr et al. Multiple sclerosis therapies differentially impact SARS-CoV-2 vaccine-induced antibody and T cell immunity and function. *JCI Insight* **7**, e156978 (2022).
58. Grant, E. J. & Gras, S. Protocol for generation of human peptide-specific primary CD8<sup>+</sup> T cell lines. *STAR Protoc.* **3**, 101590 (2022).
59. Grant, E. J. et al. Broad CD8<sup>+</sup> T cell cross-recognition of distinct influenza A strains in humans. *Nat. Commun.* **9**, 5427 (2018).
60. Brochet, X., Lefranc, M.-P. & Giudicelli, V. IMGT/V-QUEST: the highly customized and integrated system for Ig and TR standardized V-J and V-D-J sequence analysis. *Nucleic Acids Res.* **36**, W503–W508 (2008).
61. Chatzileontiadou, D. S. M., Szeto, C., Jayasinghe, D. & Gras, S. Protein purification and crystallization of HLA-A\*02:01 in complex with SARS-CoV-2 peptides. *STAR Protoc.* **2**, 100635 (2021).
62. Alamyar, E., Duroux, P., Lefranc, M.-P. & Giudicelli, V. Immunogenetics, methods and applications in clinical practice. *Methods Mol. Biol.* **882**, 569–604 (2012).
63. Bailey, T. L. & Elkan, C. Fitting a mixture model by expectation maximization to discover motifs in biopolymers. *Proc. Int. Conf. Intell. Syst. Mol. Biol.* **2**, 28–36 (1994).
64. Lefranc, M.-P. et al. IMGT®, the international ImMunoGeneTics information system® 25 years on. *Nucleic Acids Res.* **43**, D413–D422 (2015).
65. McPhillips, T. M. et al. Blu-Ice and the Distributed Control System: software for data acquisition and instrument control at macromolecular crystallography beamlines. *J. Synchrotron Radiat.* **9**, 401–406 (2002).
66. Kabsch, W. XDS. *Acta Crystallogr. D* **66**, 125–132 (2010).
67. McCoy, A. J. et al. Phaser crystallographic software. *J. Appl. Crystallogr.* **40**, 658–674 (2007).
68. Collaborative Computational Project, Number 4. The CCP4 suite: programs for protein crystallography. *Acta Crystallogr. D* **50**, 760–763 (1994).
69. Toor, J. S. et al. A recurrent mutation in anaplastic lymphoma kinase with distinct neoepitope conformations. *Front. Immunol.* **9**, 99 (2018).
70. Emsley, P., Lohkamp, B., Scott, W. G. & Cowtan, K. Features and development of Coot. *Acta Crystallogr. D* **66**, 486–501 (2010).
71. Smart, O. S. et al. Exploiting structure similarity in refinement: automated NCS and target-structure restraints in BUSTER. *Acta Crystallogr. D* **68**, 368–380 (2012).
72. Afonine, P. V. et al. Towards automated crystallographic structure refinement with phenix.refine. *Acta Crystallogr. D* **68**, 352–367 (2012).

**Acknowledgements** We thank the thousands of volunteers who donated bone marrow and who took the time to participate in this study; the staff at the Flow Cytometry facilities of La Trobe and Monash Universities; N. Faramaz for his help with the TCR sequence analysis; and D. Jayasinghe for his technical assistance. This study was funded by grants R01AI159260, 3U2CEB021881-05S1 and R21HG012386 from the National Institutes of Health; the National Health and Medical Research Council (NHMRC); Medical Research Future Fund (MRFF2005654 to S.G.); NHMRC SRF (1159272 to S.G.); and Research Training Program (RTP) stipend scholarship (to L.D.M.). The CIBMT is supported primarily by Public Health Service U24CA076518 from the National Cancer Institute (NCI), the National Heart, Lung and Blood Institute (NHLBI) and the National Institute of Allergy and Infectious Diseases (NIAID); HHS250201700006C from the Health Resources and Services Administration (HRSA); and N00014-20-1-2832 and N00014-21-1-2954 from the Office of Naval Research. Support is also provided by Be the Match Foundation, the Medical College of Wisconsin and the National Marrow Donor Program. The views expressed in this article do not reflect the official policy or position of the National Institute of Health, the Department of the Navy, the Department of Defense, Health Resources and Services Administration (HRSA) or any other agency of the US Government.

**Author contributions** J.A.H., D.G.A., S.G., D.S.M.C., L.D.M. and M.M. conceived this work. J.A.H., D.G.A., J.J.S., S.G., D.S.M.C., L.D.M., G.M.M., J.E.O., M. J. Pletcher., N.D.P. and M.M. developed the methodology. J.A.H., D.G.A., J.J.S., S.G., D.S.M.C., L.D.M. and K.G. undertook the formal analysis. J.A.H., D.G.A., J.J.S., S.G., D.S.M.C. and L.D.M. conducted the investigations. J.A.H., P.J.B., C.S., S.G., C.A.V.-G., S.R.S., D.J.L., S. Lee., M.M., G.M.M., J.E.O. and M. J. Pletcher. obtained resources. J.A.H., D.G.A., S.G., D.S.M.C., L.D.M., T.Y., N.D.P., X.B., K.K., V.W.M., V.P., S.S., F.B., G.S.G., K.L.L., C.Y., C.T.M., M. J. Peluso., R.H., T.J.H., S.G.D., M.D., S. Lu., S.A.G., J.D.K., J.N.M., C.A.V.-G., S.R.S., D.J.L., M.J.D.-O., C.S., S. Lee., G.M.M., J.E.O. and M. J. Pletcher. undertook sample collection and data curation. J.A.H., D.G.A., J.J.S., S.G., D.S.M.C., L.D.M. and M.J.D.-O. were responsible for visualization. J.A.H., S.G., D.S.M.C. and S. Lee. obtained funding. J.A.H. and S.G. conducted the project administration. J.A.H., S.G., D.S.M.C. and P.J.B. were responsible for supervision. J.A.H., D.G.A., J.J.S., S.G., D.S.M.C. and L.D.M. wrote the original draft. All of the authors reviewed and edited the final manuscript.

**Competing interests** The authors declare no competing interests.

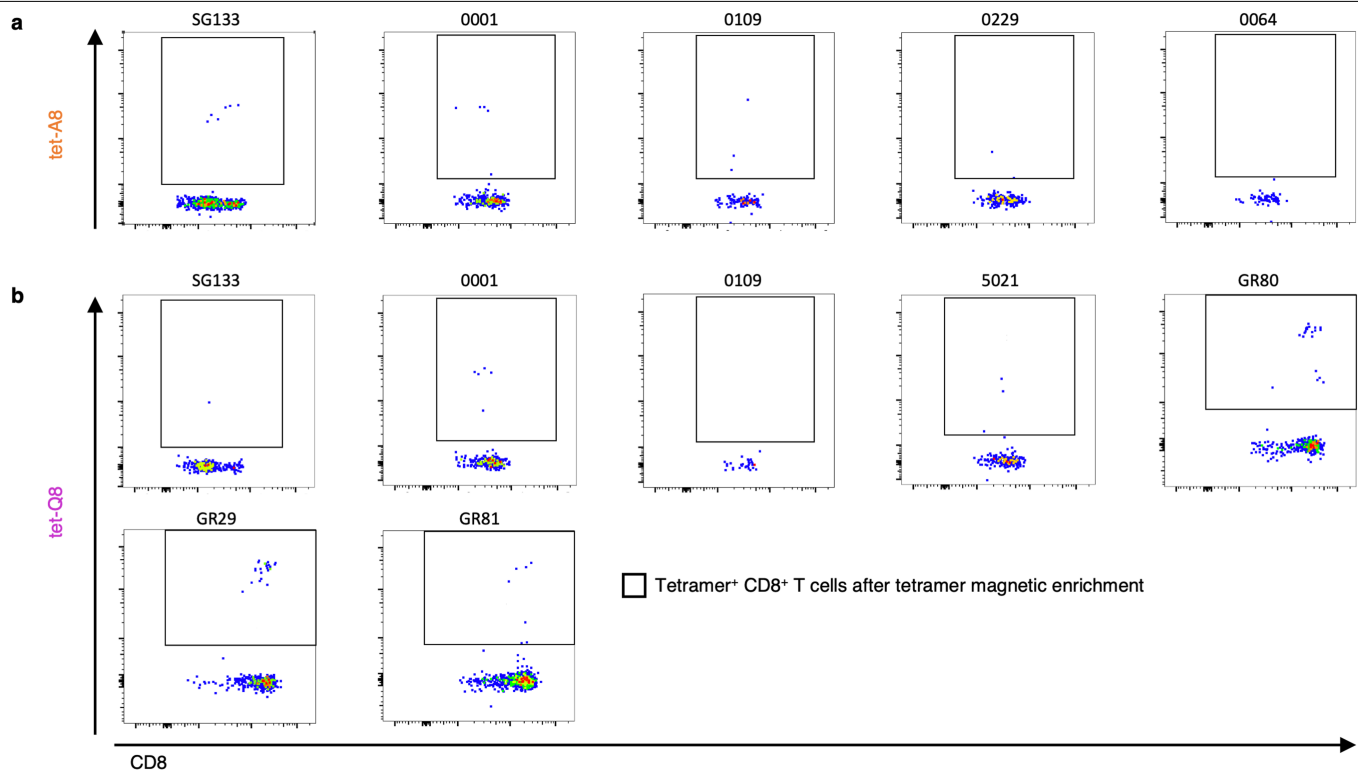
## Additional information

**Supplementary information** The online version contains supplementary material available at <https://doi.org/10.1038/s41586-023-06331-x>.

**Correspondence and requests for materials** should be addressed to Jill A. Hollenbach.

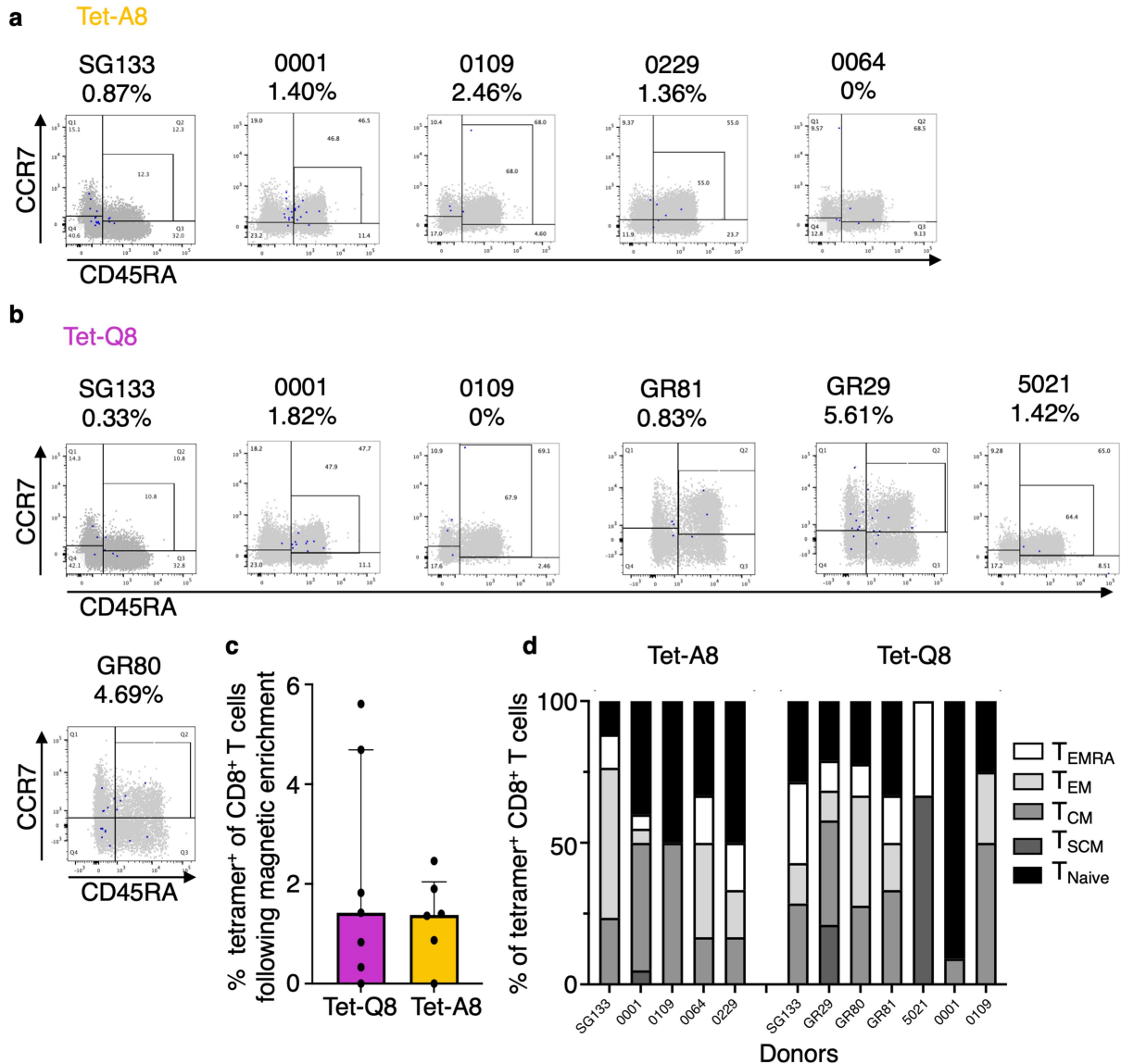
**Peer review information** *Nature* thanks Donald Vinh, Lawrence Stern and the other, anonymous, reviewer(s) for their contribution to the peer review of this work.

**Reprints and permissions information** is available at <http://www.nature.com/reprints>.



**Extended Data Fig. 1** | *Ex vivo* raw data from pre-pandemic samples from individuals carrying HLA-B\*15:01. (a–b) Individual FACS plots for each pre-pandemic donor samples used for *ex vivo* tetramer staining following

tetramer magnetic enrichment with tet-A8 tetramer (a) and with tet-Q8 tetramer (b), from 5 and 7 donors, respectively. The enriched tetramer<sup>+</sup> CD8<sup>+</sup> T cells observed are indicated within the inner square.

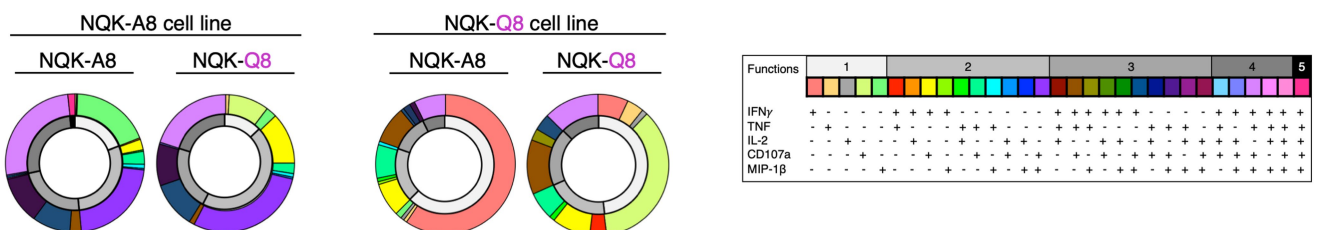


**Extended Data Fig. 2 | Ex vivo tetramer and phenotype analysis of NQK-Q8- and NQK-A8-specific T cells, related to Fig. 1d.** (a, b) FACS plots of NQK-A8-tetramer<sup>+</sup> CD8<sup>+</sup> T cells following tetramer magnetic enrichment (a) and NQK-Q8-tetramer<sup>+</sup> CD8<sup>+</sup> T cells (b). The NQK-A8- and NQK-Q8-tetramer<sup>+</sup> CD8<sup>+</sup> T cells shown as blue dots were plotted versus CD3<sup>+</sup> T cells shown as grey dots and gated on CCR7 and CD45RA to determine memory status, following tetramer magnetic enrichment for each donor. (c) The percentage of tetramer<sup>+</sup> of CD8<sup>+</sup> T cells after tetramer magnetic enrichment is reported for each donor

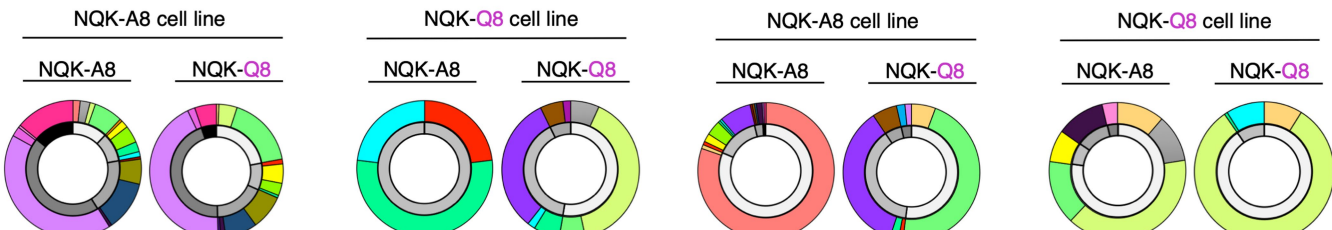
with the purple bar for the Tet-Q8 tetramer and the orange bar for the Tet-A8 tetramer ( $n = 7$  and  $n = 6$  biologically independent samples, respectively). Data are presented as median values with IQR (interquartile range). The individual percentage for each donor is indicated on panels a and b. (d) The proportion of T<sub>naive</sub> (CD45RA<sup>+</sup>CCR7<sup>+</sup>CD95<sup>-</sup>); T<sub>SCM</sub> (stem cell memory, CD45RA<sup>+</sup>CCR7<sup>+</sup>CD95<sup>+</sup>); T<sub>CM</sub> (central memory, CD45RA<sup>+</sup>CCR7<sup>+</sup>); T<sub>EM</sub> (effector memory, CD45RA<sup>+</sup>CCR7<sup>+</sup>); T<sub>EMRA</sub> (terminally differentiated, CD45RA<sup>+</sup>CCR7<sup>+</sup>) cells in different donors.

# Article

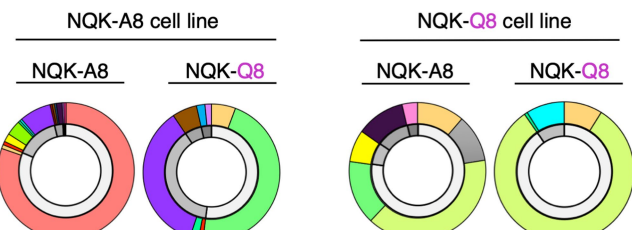
Donor GR80



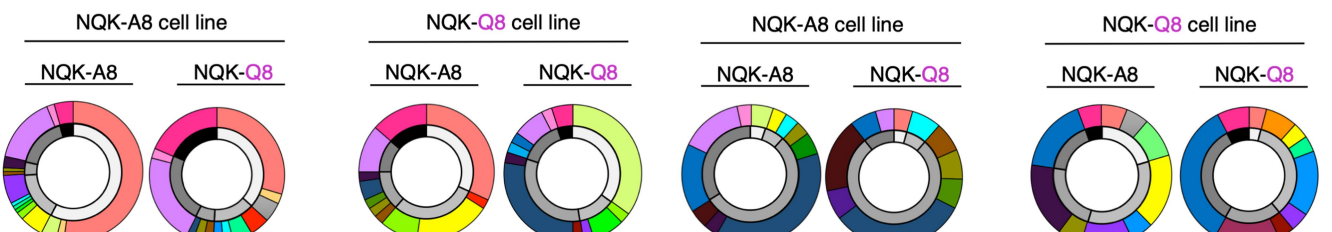
Donor GR29



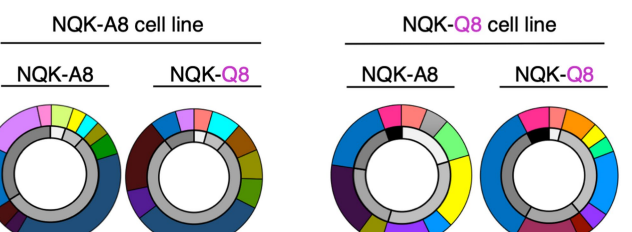
Donor GR8



Donor GR81

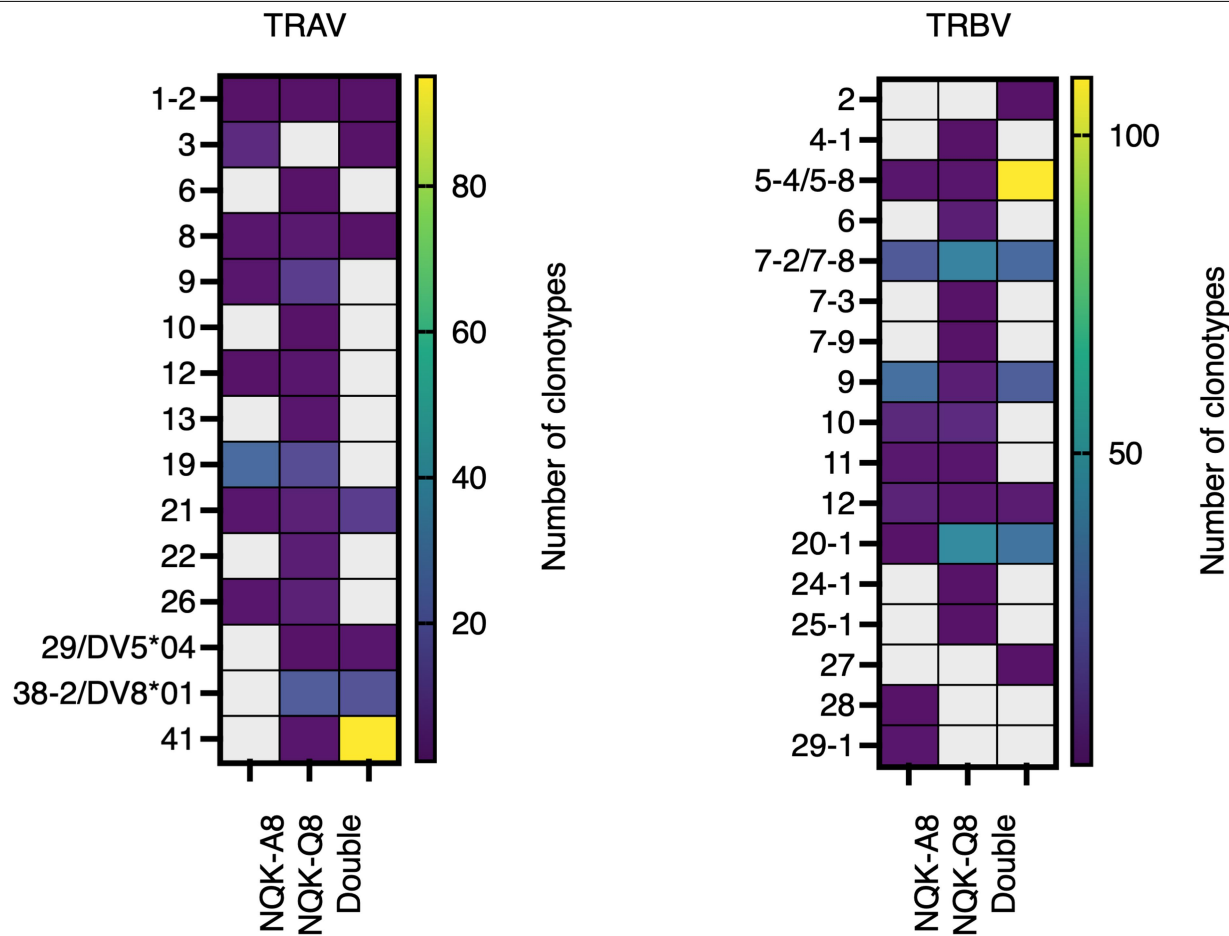


Donor SG5



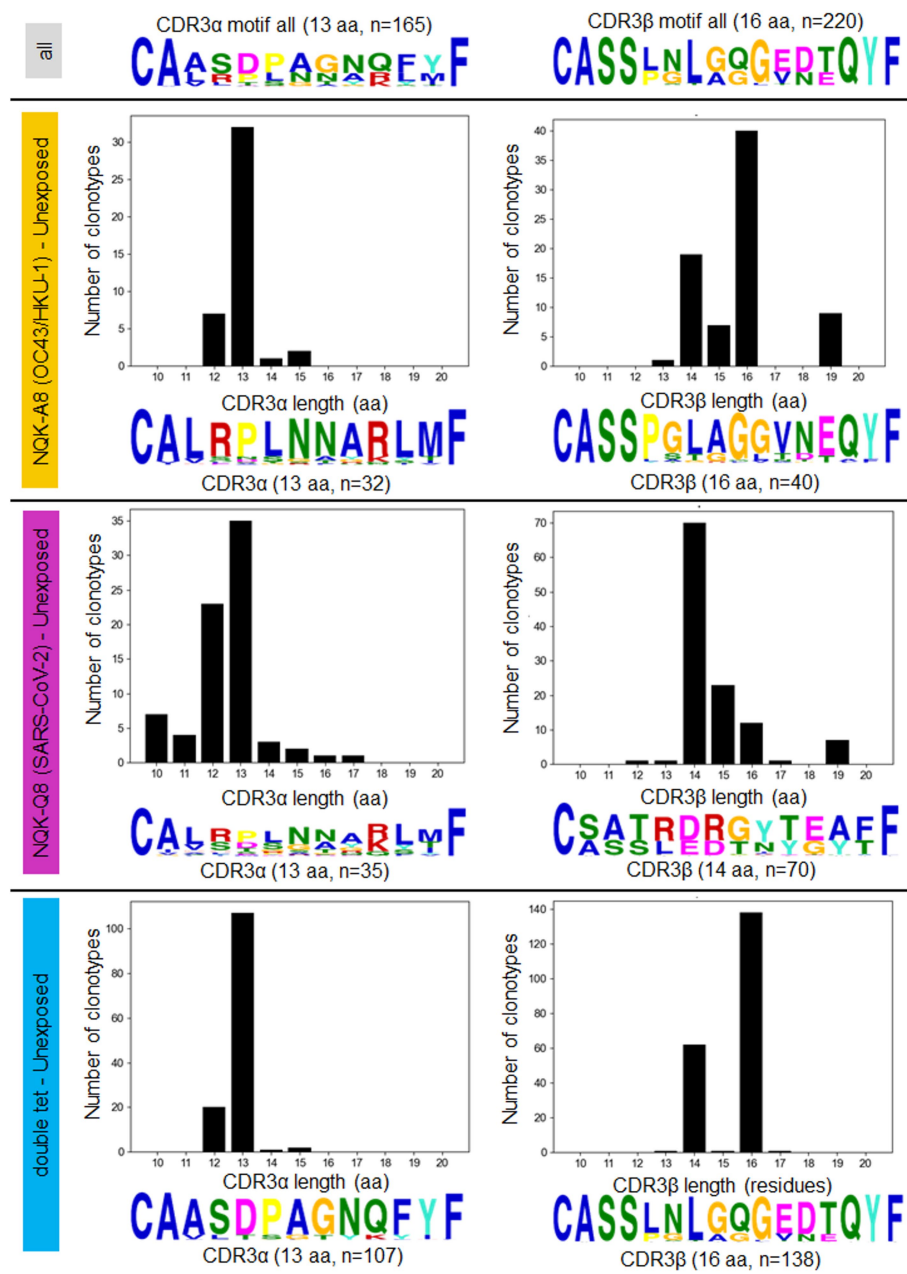
**Extended Data Fig. 3 | Functionality pie charts of T cell lines.** Frequency of CD8 $^{+}$  T cells with different effector functions (IFN $\gamma$ , TNF, IL-2, MIP-1 $\beta$ , CD107a) was determined, along with the number of different functions, minus the no

peptide control. The outer ring of the double ring pie shows the function profile in different colours according to the table, and the inner ring represents the number of functions with black for 5 and white for 1.



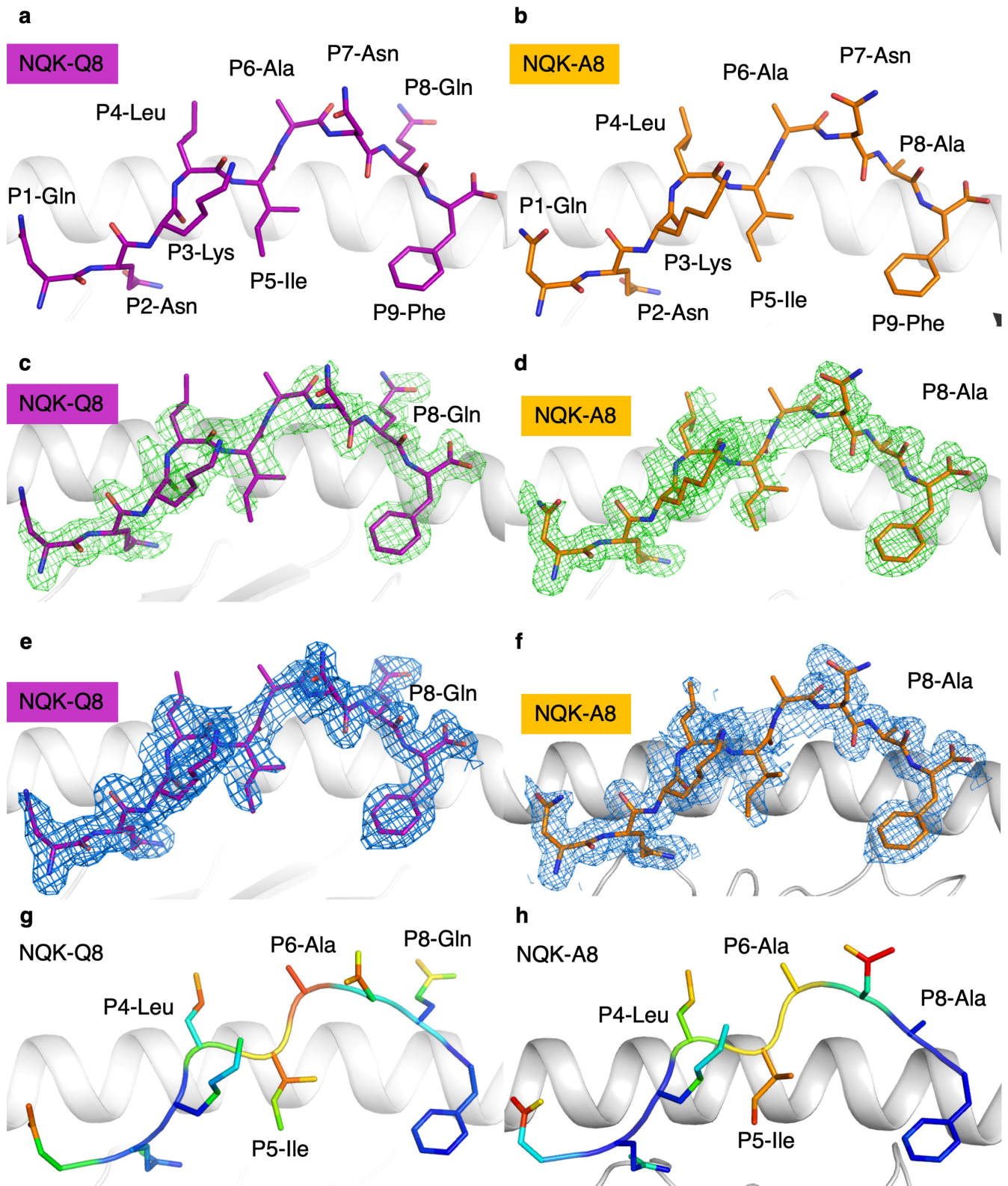
**Extended Data Fig. 4 | TRAV and TRBV usage specific for each tetramer used in unexposed individuals.** Heatmaps displaying preferred TRAV (left) and TRBV (right) usage of NQK-Q8-, NQK-A8-, or both (double) peptide-specific TCRs in all unexposed donors collectively.

# Article



**Extended Data Fig. 5 | NQK-specific TCR repertoire CDR3 analysis in unexposed donors.** Summary of CDR3 $\alpha$  (left) and CDR3 $\beta$  (right) lengths and motif analysis for the NQK-A8 (top), NQK-Q8 (middle), and both peptides (bottom)-specific TCR clonotypes in unexposed donors. The MEME motif discovery program was used to identify aa motifs enriched; the relative size of each residue symbol is proportional to its frequency, while the total height of

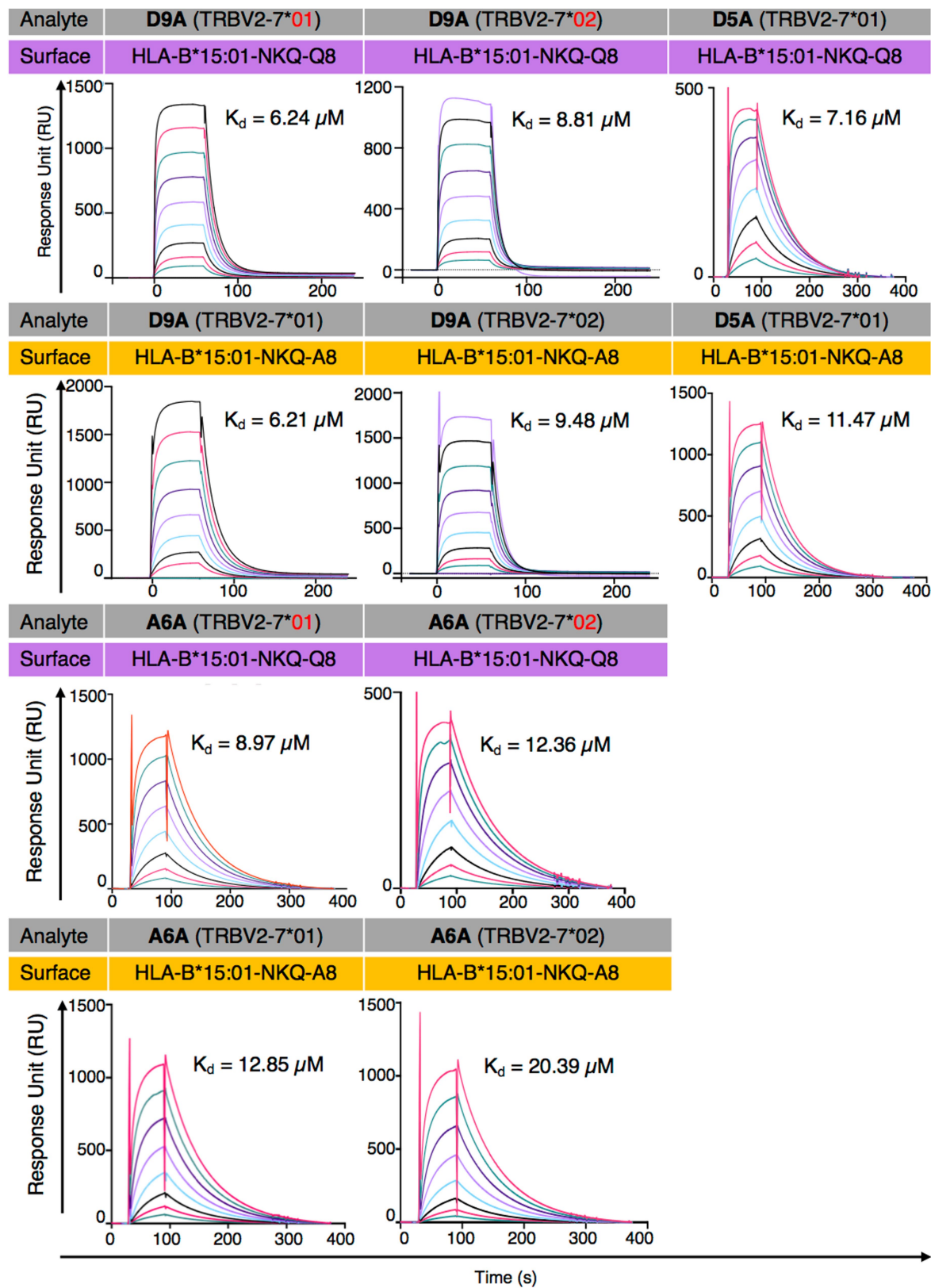
aa symbols indicates the information content of the position in bits. The motif on top left panel is the CDR3 $\alpha$  13 amino acid (aa) long sequence motif derived from all CDR3 $\alpha$  sequences obtained (n = 165); on the right top panel is the CDR3 $\beta$  16 aa long sequence motif derived from all CDR3 $\beta$  sequences obtained (n = 220).



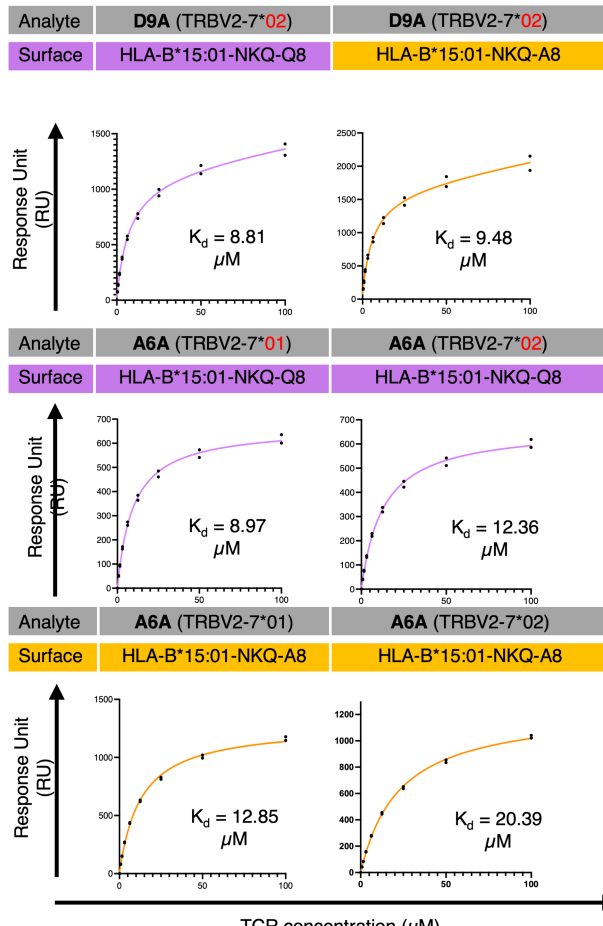
**Extended Data Fig. 6 | HLA-B\*15:01 interaction with peptides derived from SARS-CoV-2 and seasonal coronaviruses.** (a–b) Structures of HLA-B\*15:01-NQK-Q8 (peptide as purple stick) (a) and HLA-B\*15:01-NQK-A8 (peptide as orange stick) (b), with the HLA chain in white cartoon. (c–d) Electron density map around the NQK-Q8 (purple stick) and NQK-A8 (orange stick) peptides, respectively, in green at 3s for the Fo-Fc map. (e–f) Electron density

map around the NQK-Q8 (purple stick) and NQK-A8 (orange stick) peptides, respectively, in blue at 1s for the 2Fo-Fc map. (g–h)  $B_{\text{factor}}$  analysis of the atoms of the NQK-Q8 and NQK-A8 peptides, respectively. The atoms are coloured according to their  $B_{\text{factor}}$  that indicates the mobility of each atom from low (blue) to high (red).

# Article



**Extended Data Fig. 7 | Surface plasmon resonance sensograms.** SPR sensograms for the 5 tested TCRs with each curve showing different concentration of the TCR.



**Extended Data Fig. 8 | Steady-state binding curves.** Steady-state binding curve for the five tested TCRs towards HLA\*15:01-NKQ-Q8 or -A8 complex. Analytes (TCRs) flowed over immobilized HLA\*15:01-NKQ-Q8 or -A8 with a concentration range of 0 to 100  $\mu M$ .  $n = 2$  biologically independent experiments performed in duplicate, with the graph showing results from one experiment.

## Article

Extended Data Table 1 | Study population demographics

<b>Total</b>	<b>Symptomatic</b>	<b>Asymptomatic</b>	
	<b>Male</b>	<b>Female</b>	<b>Age (median, years)</b>
1,428	1,292	136	
	90.5%	9.5%	
<b>All</b>	19%	81%	34
<b>Symptomatic</b>	18%	82%	33
<b>Asymptomatic</b>	26%	74%	41

Among these respondents, 136 (9.5%) reported having remained asymptomatic for at least two weeks before and after a positive test for the virus. The median age was increased in asymptomatic compared to symptomatic individuals (asymptomatic=41, symptomatic=33,  $p < 0.001$ ), and we observed increased reporting for asymptomatic infection in males ( $p=0.02$ ). We also collected data on several diseases and conditions that might impact COVID-19 disease course. Among all individuals who reported a positive test for the virus ( $n=1,428$ ), 67% reported no known COVID-19-associated comorbidities.

Extended Data Table 2 | Data Collection and Refinement Statistics

<b>Data Collection Statistics</b>	<b>HLA-B*15:01-NQK-Q8</b>	<b>HLA-B*15:01-NQK-A8</b>
<b>Space group</b>	$P2_12_12_1$	$P2_12_12_1$
<b>Cell Dimensions (a,b,c) (Å)</b>	50.81, 81.24, 110.07	50.93, 81.55, 110.53
<b>Resolution (Å)</b>	45.56 – 1.85 (1.89 – 1.85)	46.25 – 1.65 (1.68 – 1.65)
<b>Total number of observations</b>	535056 (32820)	761967 (35727)
<b>Number of unique observations</b>	39747 (2437)	56241 (2718)
<b>Multiplicity</b>	13.5 (13.5)	13.5 (13.1)
<b>Data completeness (%)</b>	100 (100)	100 (100)
$I/s_I$	9.2 (2.6)	12.0 (2.4)
<b>Mn(I) half-set correlation <math>CC_{(1/2)}</math></b>	0.996 (0.839)	0.998 (0.728)
$R_{\text{pim}}^a$ (%)	6.1 (62.7)	4.8 (67.9)
<b>Refinement Statistics</b>		
<b>Non-hydrogen atoms</b>		
<b>Protein</b>	3229	3232
<b>Water</b>	329	510
$R_{\text{factor}}^b$ (%)	17.8	18.3
$R_{\text{free}}^b$ (%)	22.3	22
<b>Rms deviations from ideality</b>		
<b>Bond lengths (Å)</b>	0.011	0.005
<b>Bond angles (°)</b>	1.484	0.994
<b>Ramachandran plot (%)</b>		
<b>Allowed region</b>	99.75	99.75
<b>Disallowed region</b>	0.25	0.25
<b>PDB code</b>	8ELH	8ELG

<sup>a</sup> $R_{\text{p.i.m}} = S_{\text{hkl}} [1/(N-1)]^{1/2} S_i | I_{\text{hkl},i} - < I_{\text{hkl}} > | / S_{\text{hkl}} < I_{\text{hkl}} >$ <sup>b</sup> $R_{\text{factor}} = S_{\text{hkl}} | | F_o | - | F_c | | / S_{\text{hkl}} | F_o |$  for all data except ≈ 5% which were used for  $R_{\text{free}}$  calculation.

Values in parentheses are for highest-resolution shell.

## Reporting Summary

Nature Portfolio wishes to improve the reproducibility of the work that we publish. This form provides structure for consistency and transparency in reporting. For further information on Nature Portfolio policies, see our [Editorial Policies](#) and the [Editorial Policy Checklist](#).

### Statistics

For all statistical analyses, confirm that the following items are present in the figure legend, table legend, main text, or Methods section.

n/a Confirmed

- The exact sample size ( $n$ ) for each experimental group/condition, given as a discrete number and unit of measurement
- A statement on whether measurements were taken from distinct samples or whether the same sample was measured repeatedly
- The statistical test(s) used AND whether they are one- or two-sided  
*Only common tests should be described solely by name; describe more complex techniques in the Methods section.*
- A description of all covariates tested
- A description of any assumptions or corrections, such as tests of normality and adjustment for multiple comparisons
- A full description of the statistical parameters including central tendency (e.g. means) or other basic estimates (e.g. regression coefficient) AND variation (e.g. standard deviation) or associated estimates of uncertainty (e.g. confidence intervals)
- For null hypothesis testing, the test statistic (e.g.  $F$ ,  $t$ ,  $r$ ) with confidence intervals, effect sizes, degrees of freedom and  $P$  value noted  
*Give  $P$  values as exact values whenever suitable.*
- For Bayesian analysis, information on the choice of priors and Markov chain Monte Carlo settings
- For hierarchical and complex designs, identification of the appropriate level for tests and full reporting of outcomes
- Estimates of effect sizes (e.g. Cohen's  $d$ , Pearson's  $r$ ), indicating how they were calculated

*Our web collection on [statistics for biologists](#) contains articles on many of the points above.*

### Software and code

Policy information about [availability of computer code](#)

#### Data collection

Data for COVID-19 testing and symptoms in the discovery cohort was collected through a smartphone app <https://eureka.app.link/covid19/>. HLA genotyping from NGS data in the CHIRP/LIINC cohort was performed with commercial software packages: HLA Explorer V1.4 (Omixon, Budapest, Hungary) and AlloSeq Tx V471 (CareDx, Brisbane, USA). The crystallographic data were collected on the MX2 beamline at the Australian Synchrotron, part of ANSTO, Australia. The data were processed using XDS (version January 10, 2022) and the structures were determined by molecular replacement using the PHASER program (v2.8.3) from the CCP4 suite (v8.0.005) with a model of HLA-B\*15:01 without the peptide (derived from PDB ID: 5TXS). Manual model building was conducted using COOT (v0.9.8.4) followed by refinement with BUSTER (version 1.2.14) and PHENIX (1.20.1-4487). The final models have been validated and deposited using the wwPDB OneDep System. Single-cell index sorting was performed on a BD FACSaria Fusion with BD FACSDiva Software v9.0. BD FACSsymphony A3 was also used for cell acquisition with BD FACSDiva Software v9.0.

#### Data analysis

Initial testing for HLA associations was performed using the R package BIGDAWG V3.0.3 All additional association analysis was conducted in R using the base stats package as described in Methods, with the exception of the meta-analysis which used the R 'meta' package V 6.2-1. All molecular graphics representations were created using PyMOL V2.5. Post-acquisition analysis of T cells was performed using FlowJo software (v10).TRA and TRB sequences were analyzed with the software suite from the International ImMunoGeneTics (IMGT) Information System. The V(D)J gene nomenclature used is that of the IMGT database ([www.imgt.org](http://www.imgt.org)). Motifs enriched were identified with the MEME suite motif discovery software (v5.5.2.). TCR sequences were analyzed using FinchTV (Geospiza v1.5.0) and IMGT software. Additional data analysis for TCR was conducted using GraphPad Prism 9 (version 9.3).

For manuscripts utilizing custom algorithms or software that are central to the research but not yet described in published literature, software must be made available to editors and reviewers. We strongly encourage code deposition in a community repository (e.g. GitHub). See the Nature Portfolio [guidelines for submitting code & software](#) for further information.

## Data

Policy information about [availability of data](#)

All manuscripts must include a [data availability statement](#). This statement should provide the following information, where applicable:

- Accession codes, unique identifiers, or web links for publicly available datasets
- A description of any restrictions on data availability
- For clinical datasets or third party data, please ensure that the statement adheres to our [policy](#)

All HLA and phenotypic data for the Citizen Science and CHIRP/LIINC and UK cohorts are available at <http://www.hlacovid19.org/database/> public database, Project 3 Hollenbach and Project 6 Langton. The crystallographic structures are available on the Protein Data Bank (PDB) server (<https://www.rcsb.org/>) under the accession codes: 8ELG and 8ELH, for HLA-B\*15:01-NQK-A8 and HLA-B\*15:01-Q8, respectively. PDB validation reports are attached.

## Human research participants

Policy information about [studies involving human research participants and Sex and Gender in Research](#).

Reporting on sex and gender

We clearly describe data for sex and include it as a variable in our association models.

Population characteristics

We include sex and age as covariates in our association models. Our cohort was 81% female with a median age of 34. In the discovery cohort, we tested models including comorbidities known to influence risk for severe disease in COVID-19, but none were associated with asymptomatic infection, our phenotype of interest, and thus are not included in the models presented in the manuscript.

Recruitment

Discovery cohorts: Subjects were volunteer bone marrow donors with valid email addresses on file with the National Marrow Donor Program (NMDP) who were invited to participate in the study through an email outreach campaign that began in July 2020. Because the donor registry has substantially greater numbers of registrants who self-identify as White compared to other population groups, we only accrued sufficient numbers of subjects in that group for a well-powered analysis. Some self-selection bias may exist both with regard to the fact that participants who tested positive for the virus may have been more likely to respond to the survey. Likewise, the requirement for a smartphone may have proved a limitation for some potential participants. CHIRP/LIINC cohort: Participants were identified through local clinical systems (UCSF Moffitt Hospital, San Francisco General Hospital, Kaiser, California Pacific Medical Center, etc.) as well as the San Francisco Department of Public Health. After confirmation of SARS CoV-2 test results or exposure to determine eligibility, participants were asked to sign a consent form, complete a baseline visit, and schedule follow-up in-person visits.

Ethics oversight

Participation in the UCSF Citizen Science study and linking to NMDP HLA data were approved by the Institutional Review Board for the University of California, San Francisco (IRB# 17-21879 and IRB# 20-30850, respectively). All participants provided written informed consent agreeing to research and publication of research results. The CHIRP and LIINC studies were approved by the Institutional Review Board for the University of California, San Francisco, (IRB# 20-30588 and 20-30479, respectively). All participants provided written informed consent agreeing to research and publication of research results. HLA-genotyped PBMCs from the USA were stored in the National Marrow Donor Program® (NMDP)/Be The Match® Research Sample Repository (ClinicalTrials.gov protocol # NCT04920474). All individuals consented to research and publication of research results and had been previously genotyped for HLA class I and class II. Ethics approval to undertake the research for the Australian PBMCs was obtained from the QIMR Berghofer Medical Research Institute Human Research Ethics Committee (P2282) and La Trobe University Human Research Ethics Committee (HEC21097).

Note that full information on the approval of the study protocol must also be provided in the manuscript.

## Field-specific reporting

Please select the one below that is the best fit for your research. If you are not sure, read the appropriate sections before making your selection.

Life sciences

Behavioural & social sciences

Ecological, evolutionary & environmental sciences

For a reference copy of the document with all sections, see [nature.com/documents/nr-reporting-summary-flat.pdf](https://nature.com/documents/nr-reporting-summary-flat.pdf)

## Life sciences study design

All studies must disclose on these points even when the disclosure is negative.

Sample size

Our study was designed to be prospective, sample size was based on the number of subjects reporting a positive test for SARS-CoV-2 prior to the end of April 2021.

Data exclusions

We excluded subjects who self-identified as other than 'White' within the registry database, owing to insufficient numbers in these groups.

Replication

We replicated our findings in two independent patient cohorts

Randomization	Randomization was not applicable as this was a retrospective case-control study design.
Blinding	Blinding was not relevant to this study, as this was a retrospective case-control study design.

## Reporting for specific materials, systems and methods

We require information from authors about some types of materials, experimental systems and methods used in many studies. Here, indicate whether each material, system or method listed is relevant to your study. If you are not sure if a list item applies to your research, read the appropriate section before selecting a response.

Materials & experimental systems		Methods
n/a	Involved in the study	n/a
<input type="checkbox"/>	<input checked="" type="checkbox"/> Antibodies	<input type="checkbox"/>
<input type="checkbox"/>	<input checked="" type="checkbox"/> Eukaryotic cell lines	<input type="checkbox"/>
<input checked="" type="checkbox"/>	<input type="checkbox"/> Palaeontology and archaeology	<input type="checkbox"/>
<input checked="" type="checkbox"/>	<input type="checkbox"/> Animals and other organisms	<input type="checkbox"/>
<input checked="" type="checkbox"/>	<input type="checkbox"/> Clinical data	<input type="checkbox"/>
<input checked="" type="checkbox"/>	<input type="checkbox"/> Dual use research of concern	<input type="checkbox"/>
		<input checked="" type="checkbox"/> ChIP-seq
		<input type="checkbox"/> <input checked="" type="checkbox"/> Flow cytometry
		<input type="checkbox"/> <input checked="" type="checkbox"/> MRI-based neuroimaging

### Antibodies

Antibodies used	<p>Antibody Clone Fluorophore Vendor Catalog #</p> <p>CD8 SKI PE-Cy7 eBioscience 25-0087-42</p> <p>CD4 RPA-T4 PerCP-Cy5.5 BioLegend 300530</p> <p>CD14 HCD14 PerCP-Cy5.5 BioLegend 325622</p> <p>CD16 B73.1 PerCP-Cy5.5 BioLegend 360712</p> <p>CD19 HIB19 PerCP-Cy5.5 BioLegend 302230</p> <p>CCR7 G043H7 Alexa 488 BioLegend 353206</p> <p>CD45RA HI100 APC/Fire 750 BioLegend 304152</p> <p>Viability N/A eFluor 506 Invitrogen 65-0866-14</p> <p>Streptavidin N/A PE Invitrogen S866</p> <p>Streptavidin N/A APC Invitrogen S868</p> <p>Streptavidin N/A BV421 BioLegend 405225</p> <p>Streptavidin N/A PE-CF594 BioLegend 405247</p> <p>CD3 BV480 BD Biosciences 566105</p> <p>CD8 PerCP-Cy5.5 BD Biosciences 565310</p> <p>CD4 BV650 BD Biosciences 563875</p> <p>CD107 AlexaFluor488 Invitrogen 53-1079-42</p> <p>IFN-<math>\gamma</math> BV421 BD Biosciences 562988</p> <p>TNF PE-Cy7 BD Biosciences 557647</p> <p>IL2 PE BD Biosciences 559334</p> <p>MIP1<math>\beta</math> APC BD Biosciences 560686</p> <p>CD14 APCH7 BD Biosciences 560180</p> <p>CD19 APCH7 BD Biosciences 560727</p> <p>CD45RA FITC BD Biosciences 555488</p> <p>CD27 APC BD Biosciences 558664</p> <p>CCR7 PE-Cy7 BD Biosciences 557648</p> <p>CD95 BV421 BD Biosciences 562616</p> <p>PD1 BV605 BD Biosciences 563245</p>
-----------------	---

Validation	<p>All antibodies used were commercial antibodies validated by the manufacturer, as described in the links provided in the Report Summary.</p> <p><a href="https://www.thermofisher.com/antibody/product/CD8a-Antibody-clone-SK1-Monoclonal/25-0087-42">https://www.thermofisher.com/antibody/product/CD8a-Antibody-clone-SK1-Monoclonal/25-0087-42</a></p> <p><a href="https://www.biologics.com/fr-ch/products/percp-cyanine5-5-anti-human-cd4-antibody-4216">https://www.biologics.com/fr-ch/products/percp-cyanine5-5-anti-human-cd4-antibody-4216</a></p> <p><a href="https://www.biologics.com/fr-ch/products/percp-cyanine5-5-anti-human-cd14-antibody-4253">https://www.biologics.com/fr-ch/products/percp-cyanine5-5-anti-human-cd14-antibody-4253</a></p> <p><a href="https://www.biologics.com/fr-ch/products/percp-cyanine5-5-anti-human-cd16-antibody-9135">https://www.biologics.com/fr-ch/products/percp-cyanine5-5-anti-human-cd16-antibody-9135</a></p> <p><a href="https://www.biologics.com/fr-ch/products/percp-cyanine5-5-anti-human-cd19-antibody-4226">https://www.biologics.com/fr-ch/products/percp-cyanine5-5-anti-human-cd19-antibody-4226</a></p> <p><a href="https://www.biologics.com/fr-ch/products/alexa-fluor-488-anti-human-cd197-ccr7-antibody-7496">https://www.biologics.com/fr-ch/products/alexa-fluor-488-anti-human-cd197-ccr7-antibody-7496</a></p> <p><a href="https://www.biologics.com/fr-ch/products/apc-fire-750-anti-human-cd45ra-antibody-13200">https://www.biologics.com/fr-ch/products/apc-fire-750-anti-human-cd45ra-antibody-13200</a></p> <p><a href="https://www.bdbiosciences.com/content/bdb/parts/generate-tds-document.nz.566105.pdf">https://www.bdbiosciences.com/content/bdb/parts/generate-tds-document.nz.566105.pdf</a></p> <p><a href="https://www.bdbiosciences.com/content/bdb/parts/generate-tds-document.ca.565310.pdf">https://www.bdbiosciences.com/content/bdb/parts/generate-tds-document.ca.565310.pdf</a></p> <p><a href="https://www.bdbiosciences.com/content/bdb/parts/generate-tds-document.ca.563875.pdf">https://www.bdbiosciences.com/content/bdb/parts/generate-tds-document.ca.563875.pdf</a></p> <p><a href="https://www.thermofisher.com/document-connect/document-connect.html?url=https://assets.thermofisher.com/TFS-Assets%2FLSG%2FCertificates-of-Analysis%2F53-1079-42_2076068.PDF">https://www.thermofisher.com/document-connect/document-connect.html?url=https://assets.thermofisher.com/TFS-Assets%2FLSG%2FCertificates-of-Analysis%2F53-1079-42_2076068.PDF</a></p> <p><a href="https://www.bdbiosciences.com/content/bdb/parts/generate-tds-document.ca.562988.pdf">https://www.bdbiosciences.com/content/bdb/parts/generate-tds-document.ca.562988.pdf</a></p> <p><a href="https://www.bdbiosciences.com/content/bdb/parts/generate-tds-document.ca.557647.pdf">https://www.bdbiosciences.com/content/bdb/parts/generate-tds-document.ca.557647.pdf</a></p> <p><a href="https://www.bdbiosciences.com/content/bdb/parts/generate-tds-document.ca.559334.pdf">https://www.bdbiosciences.com/content/bdb/parts/generate-tds-document.ca.559334.pdf</a></p>
------------	--

<https://www.bdbiosciences.com/content/bdb/paths/generate-tds-document.ca.560686.pdf>  
<https://www.bdbiosciences.com/content/bdb/paths/generate-tds-document.ca.560180.pdf>  
<https://www.bdbiosciences.com/content/bdb/paths/generate-tds-document.ca.555488.pdf>  
<https://www.bdbiosciences.com/content/bdb/paths/generate-tds-document.ca.558664.pdf>  
<https://www.bdbiosciences.com/content/bdb/paths/generate-tds-document.ca.557648.pdf>  
<https://www.bdbiosciences.com/content/bdb/paths/generate-tds-document.ca.562616.pdf>  
<https://www.bdbiosciences.com/content/bdb/paths/generate-tds-document.ca.563245.pdf>

## Eukaryotic cell lines

Policy information about [cell lines and Sex and Gender in Research](#)

Cell line source(s)	The CD8+ T cell lines were generated from Peripheral blood mononuclear cells (PBMCs) that were separated from whole blood or buffy coats from donors using density gradient centrifugation.
Authentication	Cell lines were not authenticated
Mycoplasma contamination	The cell lines were not tested for mycoplasma contamination
Commonly misidentified lines (See <a href="#">ICLAC</a> register)	N/A

## Flow Cytometry

### Plots

Confirm that:

- The axis labels state the marker and fluorochrome used (e.g. CD4-FITC).
- The axis scales are clearly visible. Include numbers along axes only for bottom left plot of group (a 'group' is an analysis of identical markers).
- All plots are contour plots with outliers or pseudocolor plots.
- A numerical value for number of cells or percentage (with statistics) is provided.

### Methodology

Sample preparation	A total of 20 unexposed and 1 triple vaccinated (VAC62) donors were recruited with all the details listed in Supplementary Table S19. PBMC were separated from whole blood or buffy coats using density gradient centrifugation. PBMC were used fresh or were cryogenically stored until use. HLA-genotyped PBMCs from the USA were stored in the National Marrow Donor Program® (NMDP)/Be The Match® Research Sample Repository (ClinicalTrials.gov protocol # NCT04920474) that had been collected from healthy donors prior to the start of the COVID-19 pandemic.
Instrument	BD LSR Fortessa and BD FACSymphony A3
Software	BD FACSDiva was used for sample collection. Cells were single-cell index sorted using a BD Aria Fusion with FACSDiva software. FlowJo 10.7.1 and 10.8.1 were used for sample analysis.
Cell population abundance	An aliquot of PBMCs was used for cell surface staining and counting with 123count eBeads (Invitrogen). The remaining PBMCs were stained with the indicated tetramer pools and enriched using anti-PE magnetic microbeads (Miltenyi) over a magnetic column, cell-surface stained, and counted as for pre-enrichment.
Gating strategy	CD8+ T cells were identified by gating of live singlet CD8+ lymphocytes that were negative for CD4/CD14/CD16/CD19. A stringent tetramer gating strategy was employed whereby CD8+ T cells labeled with only two fluorophores were considered antigen-specific. TAME:CD8+ T cells were identified by gating of live singlet CD8+ lymphocytes that were negative for CD4/CD14/CD16/CD19 . A stringent tetramer gating strategy was employed whereby CD8+ T cells labeled with only two fluorophores were considered antigen-specific. Memory status of tetramer-positive CD8+ T cells was determined by lack of CCR7 and CD45RA co-expression.

- Tick this box to confirm that a figure exemplifying the gating strategy is provided in the Supplementary Information.